

A methodology to compare sea-level index points and sea-level models



Juan Sebastian Garzón Alvarado

Institute for Geoinformatics

Westfälische Wilhelms-Universität Münster

Dissertation supervised by:

Prof. Dr. Edzer Pebesma
Institute for Geoinformatics
University of Münster

Prof. Dr. Alessio Rovere
University of Venice

A thesis submitted for the degree of

Master of Science Geoinformatics

2021

Declaration of Academic Integrity

I hereby confirm that this thesis on *A methodology to compare sea-level index points and sea-level models* is solely my own work and that I have used no sources or aids other than the ones stated. All passages in my thesis for which other sources, including electronic media, have been used, be it direct quotes or content references, have been acknowledged as such and the sources cited.

Münster, January 21, 2022

I agree to have my thesis checked in order to rule out potential similarities with other works and to have my thesis stored in a database for this purpose.

Münster, January 21, 2022

Acknowledgements

I want to thank different people that supported different stages of this project. Thanks to my supervisors, Prof. Rovere, and Prof. Pebesma, for their comments and guidance during the project. Special thanks to Prof. Rovere for his guidance in the process of exploring sea-level research as a field during the last year. Thanks to Prof. Verstegen, Prof. Kray, and Daniel Nüst for their dedication in their classes and projects at IFGI, which allowed me to learn and implement different ideas to this project. Thanks to Dr. Jackqueline Austermann from Columbia University for sharing the GIA model output. Thanks to Eeva Langeveld for her valuable comments on the final manuscript.

The data used in this study was extracted from WALIS, a sea-level database interface developed by the ERC Starting Grant “WARMCOASTS” (ERC-StG-802414), in collaboration with PALSEA (PAGES / INQUA) working group. The database structure was designed by A. Rovere, D. Ryan, T. Lorscheid, A. Dutton, P. Chutcharavan, D. Brill, N. Jankowski, D. Mueller, M. Bartz, E. Gowan, and K. Cohen.

Juan Sebastian Garzón
January 21, 2022

Abstract

Sea-level change studies in geological time scales require integrating multiple research methods with different characteristics and contexts. This work presents a methodology to compute and analyze the residual value between the relative sea level recorded on field observations (sea level indicators) and the results of earth and ice models predicting the glacial isostatic adjustment (GIA) phenomena during the last 200 ka. The method relies on an initial Monte Carlo sampling of the temporal (age) and relative sea level parameters of sea-level indicators using the World Atlas of Last Interglacial Shorelines (WALIS) dataset. Subsequently, the proposed method compares the age and relative sea level values with a selection from 216 GIA models with five different parameters. The document includes the explanation and code implementation of the method using a reproducible R workflow and a series of tests to evaluate the results. The document presents two cases studying the residual values along the passive South American Atlantic margin and the active Pacific margin. Results show higher residual values for the active South American Pacific margin than the passive Atlantic from 125 to 75 ka. Comparison within each region shows no significant differences in the residual values along each coast. Results analysis and the data context suggest that direct comparison of mean residual is unsuitable for evaluating regional differences. In this regard, GIA model parameters only seem to influence different residual values in the active Pacific margin. However, alternative explanations unrelated to geological phenomena are discussed to explain these differences. The limitations and challenges to comparing residual values are discussed, including different interpretations for the residual results. Finally, this work suggests a series of steps to expand the integration of sea-level research data.

Contents

List of Figures	vii
List of Tables	viii
List of Abbreviations	ix
1 Introduction	1
2 Theoretical framework	5
2.1 Sea level and relative sea level	5
2.2 Sea-level indicators	7
2.3 Sea-level indicators types	9
2.4 Sea-level deterministic models	11
3 Methodology	14
3.1 Extraction of distribution parameters	14
3.2 Merging sea-level indicators	19
3.3 GIA models as a data cube	21
3.4 Residual calculation	22
3.5 Curve fitting	22
3.6 Evaluation - Case studies	23
3.7 Methodology reproducibility	24
4 Results	26
4.1 South American Atlantic coast (5-55° S)	26
4.2 South American Pacific coast (1°N-40°S)	32
5 Discussion	39
5.1 South American Atlantic coast	39
5.2 South American Pacific coast	41
5.3 Sampling methods	43

Contents

6 Conclusions	46
References	49

List of Figures

2.1	Diagram of relative sea level changes	6
3.1	Ranges for uniform distribution sampling	16
3.2	Sea-level indicators sampling	20
3.3	Diagram of limiting data merging	20
3.4	GIA model example	21
3.5	Diagram of Residual computation from SLI and GIA models	23
4.1	South American Atlantic coast - Regions and sea-level indicators location	27
4.2	South American Atlantic coast - GIA models and SLIP point cloud	28
4.3	South American Atlantic coast - Residual values	29
4.4	South American Atlantic coast - Mean residual values by grouping parameters	30
4.5	South American Atlantic coast - Mean residual values by region	32
4.6	South American Pacific coast - Regions and sea-level indicators location	33
4.7	South American Pacific coast - GIA models and SLIP point cloud	34
4.8	South American Pacific coast - Residual values	36
4.9	South American Pacific coast - Mean residual values by grouping parameters	37
4.10	South American Pacific coast - Mean residual values by region	38

List of Tables

3.1	Extraction of Age parameters for SLIPs	15
3.2	Extraction of Age parameters for SLIPs with uniform sampling around sea level peaks.	17
3.3	Extraction of RSL parameters for single corals indicators	17
3.4	Extraction of RSL parameters for sea-level indicators	18
3.5	Extraction of RSL parameters for limiting indicators	18
3.6	GIA models parameters	22
3.7	WALIS References by case study	25
4.1	South America Atlantic coast - Number of SLIPs by subregion . . .	27
4.2	South America Atlantic coast - Kruskal test	31
4.3	South America Atlantic coast - Pairwise Wilcox test	31
4.4	South America Pacific coast - Number of SLIPs by subregion . . .	34
4.5	South America Pacific coast - Kruskal test	36
4.6	South America Pacific coast - Pairwise Wilcox test	38

List of Abbreviations

GIA	Glacial Isostatic Adjustment
IR	Indicative Range
LIG	Last Interglacial period
MIS	Marine Isotope Stages
RSL	Relative Sea Level
RWL	Reference Water Level
SLI(s)	Sea-level Indicator(s)
SLIP(s)	Sea-level index point(s)
WALIS	World Atlas of Last Interglacial Shorelines

1

Introduction

Discussions about the importance of sea-level changes and their causes and consequences are common in academic and non-academic spaces. Modern monitoring of sea-level changes using satellite observation and tide gauges provides an increasing influx of information to record and analyze the real-time evolution of this phenomenon (see Shennan, 2015). However, as pointed by Shennan (2015), understanding sea-level changes require information beyond modern techniques to identify long trends driving changes in sea level. For example, the study of long-term sea-level changes improves the ability to predict the consequences of a warmer world by comparing with periods with similar conditions such as the Marine Isotope Stage 5e (MIS-5e) (128-118 ka) (Rovere et al., 2019). Scientists use different techniques and approaches to estimate relative sea level changes for studies in such timescales (thousands to hundred thousands of years). First, the measurement, dating, and proxy reconstruction of sea-level indicators (SLIs) allow researchers to determine the vertical elevation of the past sea level in a specific location and time. Researchers in that area are commonly referred to as ‘geology-oriented’ or ‘field-oriented’ (see Shennan, 2015; Milne, 2015) as their work relies on *in situ* observations and measurements. Second, researchers use computational modeling (i.e., modeling community) to simulate global, regional, and local dynamics of drivers of sea-level changes. Combining the techniques used by both communities allows researchers to understand better the dynamics that control sea-level changes at timescales more prolonged than those usually covered by tide gauges or satellite altimetry data.

Even though proxy reconstruction (sea-level indicators) and modeling of sea-level

1. Introduction

changes address the same problem, there are multiple challenges to integrating their results. First, sea-level indicators (SLIs) and models result from two different research communities, so integration in a shared reference frame is required. Shennan (2015) points to some challenges for this integration. For example, the two communities have different (and multiple) definitions of relevant terms as sea level and relative sea level. Second, sea-level indicators result from various techniques with different age and relative sea level (RSL) uncertainties.

For this reason, statistical methods need to be employed to compare SLIs with a deterministic model. Ashe et al. (2019) mention integration challenges for SLIs data into statistical methods, for example, the non-Gaussian nature of some of its features and the temporal uncertainties of the data. Additionally, multiple authors mention the importance of improving the standardization of SLIs data to guarantee correct use of data to build, interpret and compare with deterministic models (see Shennan, 2015; Ashe et al., 2019; Hijma et al., 2015). In summary, the different origins and characteristics of sea-level indicators (SLIs) and sea-level models complicate data integration.

In this context, this project aims to investigate the relationship between relative sea level recorded by sea-level indicators (SLIs) and the modeled glacial isostatic adjustment (GIA) process. Specific objectives of this project consist of developing tools to extract SLIs from a standardized data set and GIA values from available models and compare them using a random sampling approach for their temporal and RSL parameters. Despite recent efforts for SLIs standardization (see Hijma et al., 2015; Rovere et al., 2019) and multiple methods for statistical analysis of SLIs (see Ashe et al., 2019), there is a knowledge gap on how to integrate results from large databases of sea-level indicators and deterministic physical models in a way that facilitates its management and discussion. The significance of this approach is that it provides sea-level researchers from both geology-oriented and modeling communities tools to explore, integrate, understand and discuss their research results in a way that guarantees better traceability of their data and methods.

There have been increasing efforts within the modeling community to promote sharing information with other research communities. Milne (2015) points to the importance of making model output available for the geology-oriented community (i.e., field community) to stimulate the interaction of sea-level researchers. Sharing research output is a challenge as models are typically hundreds of large files hard to share with other researchers without proper technical infrastructure. However, some recent and continuous efforts show advances to overcome these technical

1. Introduction

barriers. For example, Prof. W.R Peltier from the University of Toronto regularly publishes updated versions of Ice Sheet Thickness and Paleotopography models (e.g., ICE-5G Peltier, 2004) relevant for sea-level modeling. Similarly, Spada and Melini (2019) published *Selen*⁴, an open-source FORTRAN program to model the glacial isostatic adjustment (i.e., one of the drivers of sea-level changes) that allows other researchers to reproduce the models' output in different machines. Other practices in the community include uploading information into data repositories (e.g., Zenodo) or sharing upon request using private servers.

Within the geology-oriented community, there are also efforts to promote standardization practices and sharing of information with other communities. For example, Hijma et al. (2015) propose a database structure that stores the sea-level indicators parameters allowing different researchers to understand the origin and details of their measurements and reproduce the process to extract their temporal (age) and relative sea-level components (RSL). Rovere et al. (2019) presents a more recent SLI standardization effort called the World Atlas of Last Interglacial Shorelines (WALIS). This database structure serves as a standard for a compilation effort of SLI for a Special Issue in the *Earth System Science Data journal*. Adopting the WALIS database structure (see Rovere et al. (2020)) resulted in more than 4.000 sea-level indicators (SLIs) available in different Zenodo repositories.

The availability of new standardized SLIs data and sea-level models outputs promotes further integration on bigger scales than previous studies. Even though the comparison between SLIs and models is an established practice since the comparison of sea-level ‘observations’ (i.e., sea-level indicators) and GIA models to access the quality of the latter published by Clark et al. (1978), their integration is not constraint to a single approach and could vary depending on the context and objective of the study. For example, in the errors-in-variables integrated Gaussian processes proposed by Cahill et al. (2015), relative sea level values from SLIs are corrected using GIA values from physical models to estimate rates of sea-level changes. These examples show that integrating SLIs and models could serve different purposes.

This work presents a method for comparing sea-level indicators from a series of glacial isostatic adjustment (GIA) models. The method computes the subtraction between the sea levels indicators and the GIA models that result in a ‘residual’ (ε) value. This study will present a methodology test using two case studies along the South American coast. The first area corresponds to the Atlantic passive tectonic margin from Brazil to Argentina and the second the active tectonic margin

1. Introduction

from Ecuador to Chile. The study's central hypothesis is that residual values are higher along the active tectonic Pacific coast than the passive Atlantic margin. An additional hypothesis is that mean residual values from different sub-regions in these margins vary due to regional geological characteristics. This work compares fitted curves and mean-residual values from each region to test the hypotheses.

2

Theoretical framework

Comparing sea-level indicators (SLIs) and glacial isostatic adjustment (GIA) models requires an understanding of different elements of sea-level research. The following section presents the state-of-the-art of SLIs and GIA models and summarizes the definitions of standard terms and mathematical relationships between the different elements required for the following chapters. Different chapters of the *Handbook of sea-level research* edited by Shennan et al. (2015) are used as main references.

2.1 Sea level and relative sea level

Following the definition proposed by Mitrovica and Milne (2003) and the notation suggested by Shennan (2015), *sea level (SL)* is the distance between the geoid (**G**) and the solid surface (**R**) for a geographic location φ at a time t (see Figure 2.1). The following equations proposed by Mitrovica and Milne (2003) summarize the relationship between these parameters and their relative movement through time:

$$SL(\varphi, t) = G(\varphi, t) - R(\varphi, t) \quad (2.1)$$

$$\Delta SL(\varphi, t) = \Delta G(\varphi, t) - \Delta R(\varphi, t) \quad (2.2)$$

with

$$\Delta G(\varphi, t) = G(\varphi, t) - G(\varphi, t_0) \quad (2.3)$$

$$\Delta R(\varphi, t) = R(\varphi, t) - R(\varphi, t_0) \quad (2.4)$$

where t_0 is a reference time.

2. Theoretical framework

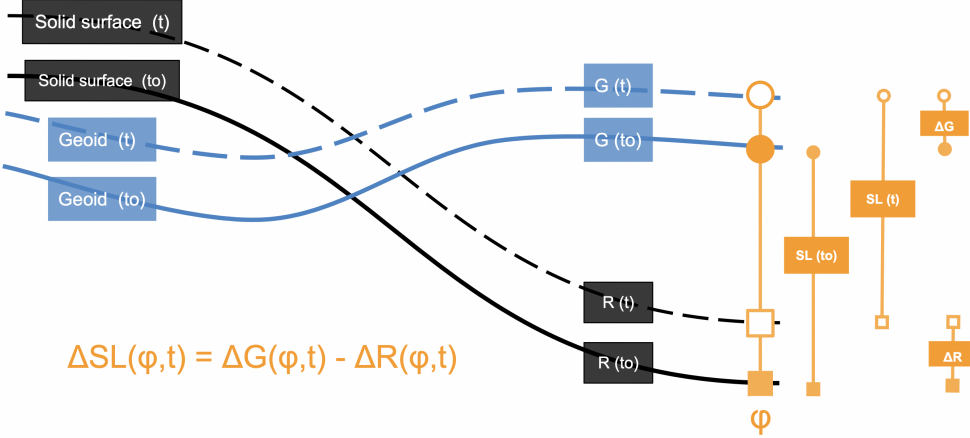


Figure 2.1: Relative sea level changes and their relationship with geoid (G) and solid surface (R) relative movements.

Shennan (2015) explains that the common practice is to calculate the change on SL relative to the present for recent time scales. Consequently:

$$RSL(\varphi, t) = SL(\varphi, t_{past}) - SL(\varphi, t_{present}) \quad (2.5)$$

Changes on the geoid **G**, the solid surface **R**, and their relative position result from the interaction of multiple earth processes with different regional and temporal extents. Shennan (2015) summarizes RSL changes and their underlying changes in the geoid and the surface with the following equations:

$$\begin{aligned} \Delta RSL(\varphi, t) = & \Delta EUS(t) + \Delta ISO(\varphi, t) + \Delta TECT(\varphi, t) \\ & + \Delta LOCAL(\varphi, t) + \Delta UNSP(\varphi, t) \end{aligned} \quad (2.6)$$

with $\Delta EUS(t)$ as eustatic changes, $\Delta ISO(\varphi, t)$ as isostatic changes, $\Delta TECT(\varphi, t)$ as tectonic changes, $\Delta LOCAL(\varphi, t)$ as local changes and $\Delta UNSP(\varphi, t)$ as unspecified changes.

Eustatic changes ($\Delta EUS(t)$) are the combination of processes that affect the mass or volume of water in the oceans resulting in global variations of sea level (see Shennan, 2015; and Rovere et al., 2016b). Unlike the other factors in Equation (2.6), eustatic changes are by definition not spatially dependent (φ) as their net variations are uniform around the globe. Some eustatic processes include changes in water mass due to melting or accumulation of ice, redistribution of water sources (not ice-related), or changes in water volume due to density variations in response to temperature changes (Rovere et al., 2016b). Beyond the global sea-level changes

2. Theoretical framework

due to the eustatic process, water mass and distribution changes trigger other non-eustatic changes.

Other parameters from equation (2.6) respond to multiple processes in different spatial and temporal ranges. The isostatic component ($\Delta ISO(\varphi, t)$) is an example of sea-level changes that respond to the eustatic process. This factor includes the effect of the glacial rebound process (i.e., glacial isostatic adjustment) in response to changes in ice and water load over the lithosphere, gravitation effects, and changes due to rotational effects resulting from ice and water redistribution (Shennan, 2015). In contrast, sea-level changes due to tectonic processes ($\Delta TECT(\varphi, t)$) are not associated with eustatic changes. This factor includes vertical changes in various time scales due to tectonic forces resulting in interseismic uplift or coseismic subsidence (Rovere et al., 2016b). Local changes ($\Delta LOCAL(\varphi, t)$) as defined by Shennan (2015) include variations due to tidal regime ($\Delta TIDE(\varphi, t)$) and sedimentation processes ($\Delta SED(\varphi, t)$). The importance of these processes is that they have high spatial variability in response to local characteristics and processes (e.g., geological, biological, and human-driven) that result in different rates of important sea-level change drivers as sediment compaction (Rovere et al., 2016b). Lastly, $\Delta UNSP(\varphi, t)$ correspond to any external factor that can not be quantified. As mentioned Shennan (2015), under specific conditions (e.g., region or time), one or more of these factors can be considered negligible.

2.2 Sea-level indicators

To perform studies in geological time scales, researchers use sea-level indicators as tools to infer previous relative sea level (RSL) and their variation through time. An SLI is a collection of evidence and interpretation of preserved features that estimate paleo-sea levels by defining four parameters: location, age, elevation, and tendency (Shennan, 2015). Sources of evidence include sedimentary, fossil, and archaeological material of an area (Shennan, 2015). As the determination of location, age, elevation, and the tendency of an SLI requires the combination of interpretations of multiple features, it is considered the result of proxy reconstruction methods rather than observations of sea level (Shennan, 2015).

The core information of an SLI can be summarized in a short phrase:

Sea level 10.000 years ago (Age) at this beach (location) was 3 meters above/below (RSL) current sea level

However, the context of the final numeric parameters (Age and RSL) consist of

2. Theoretical framework

the details of the preserved features, the combination of results of different techniques, and the interpretations of these features with their errors and uncertainties (see Shennan, 2015; Hijma et al., 2015). Hijma et al. (2015) proposes a sea-level database structure to store the required context information for the SLIs and avoid erroneous inferences. This information includes details about the samples (evidence), dating techniques (age), elevation measurements, datum, and error of measurements. With a similar approach, Rovere et al. (2020) propose the World Atlas of Last Interglacial Shorelines (WALIS) as a database structure focused on SLIs from around 130 ka. The database structure preserves the most relevant information taking into account usual methods used to measure the different parameters of SLIs (e.g., most common Quaternary dating methods) (see Rovere et al., 2019).

In the following sections, the Age and Elevation parameters of an SLI will be explained using the WALIS notation and focusing on the essential features for the Last Interglacial.

2.2.1 Age parameter

The age parameter of an SLI results from the combination of absolute and relative dating processes available from the material (e.g., rock samples). In the database structure proposed by Rovere et al. (2020), there are six dating techniques categories: *uranium-thorium series (U-Series)*, *Amino acid racemization (AAR)*, *Electron spin resonance dating (ESR)*, *Luminescence*, *Stratigraphic constraint* and *others*. Age calculation resulting from these techniques consists of two groups: (1) Radiometric ages (Absolute) and (2) temporal constraints (Relative). Radiometric dating techniques for samples during the last interglacial (128–116 ka) are predominantly U-Series, Luminescence, and ESR (Rovere et al., 2016a). Datings results are usually reported with 1-sigma errors ranging from 0.5 to 20 ka. Relative dating techniques such as AAR or stratigraphic constraints result in temporal ranges (upper and lower age) defined by known subdivisions of geologic time. In general, these techniques allow distinguishing from interglacial periods (Rovere et al., 2016a). An essential feature from the WALIS database structure is that an SLI could have more than one Age constraint. That is possible as the SLI material may allow multiple observations (e.g., more than one distinct type of fossil) or multiple dating techniques.

2. Theoretical framework

2.2.2 Elevation parameter

The elevation parameter (paleo RSL) of an SLI represents its formation position relative to tide levels under the assumption that this distance is constant (Hijma et al., 2015). For a sample (s), the RSL parameter results from the following equations:

$$RSL = RWL - E_s \quad (2.7)$$

with Reference Water level (RWL) as the middle point of the range over which an indicator forms (i.e., Indicative Range) and E_s its current elevation relative to tide levels (see Hijma et al., 2015). The definition of an Indicative range (IR) for a sample depends on the characteristics of the indicator, and there are multiple methods to define it. One example is by direct comparison with modern elevation distributions (see Woodroffe and Barlow, 2015). These two parameters (i.e., RWL and IR) are the *indicative meaning* of sea-level indicators. Rovere et al. (2016a) summarize a series of formulas to calculate RWL , IR , and their uncertainty from modern analogs:

$$RWL = \frac{U_l + L_l}{2} \quad (2.8)$$

$$IR = U_1 - L_1 \quad (2.9)$$

$$\delta_{RSL} = \sqrt{E_e^2 + \left(\frac{IR}{2}\right)^2} \quad (2.10)$$

with U_l and L_l being the upper and lower limit of the modern analog, δ_{RSL} the RSL uncertainty, and E_e the standard deviation of the elevation measurement.

The resulting relative sea level parameter (RSL) is not necessarily a bounded interval, but it could also be an unbounded interval at one of its limits. As pointed out by Rovere et al. (2016a), some indicators do not provide the evidence to quantify the position relative to a tide level, but a relative position can be derived. For example, a sample with freshwater origin does not have a direct tide level equivalency, but it indicates the relative sea level position (Hijma et al., 2015).

2.3 Sea-level indicators types

Depending on the combination of Age and RSL parameters, SLIs can be classified either as limiting indicators or sea-level index points (SLIPs).

2. Theoretical framework

2.3.1 Limiting indicators

Limiting data points are the indicators with an unknown *indicative meaning* that can not be associated with a past tide level (i.e., unbounded interval) (see Hijma et al., 2015). Depending on the characteristics of the sea-level indicators, they can be either lower or upper limiting data points. For example, marine organisms with uncertain vertical living ranges are lower limiting data points (or marine limiting), and freshwater samples are upper limiting data points (or terrestrial limiting) (see Hijma et al., 2015). In short, marine limiting indicates that the RSL was *above* certain level, and terrestrial limiting that the RSL was *below* that position.

2.3.2 Sea level index point

Contrary to limiting data, sea-level index points (SLIPs) are indicators with a known *indicative meaning* that can be associated with a past tide level (i.e., bounded RSL interval) (see Hijma et al., 2015). Rovere et al. (2020) explicitly differentiate SLIPs and limiting indicators in their proposed database structure and include for SLIPs the upper (U_l) and lower (L_l) limits of the modern analog. As these parameters are known, Equation (2.9) applies to SLIPs. The Age parameter of a SLIP can result either from absolute or relative dating methods, and its graphic representation is a range with the error of the technique (Rovere et al., 2020).

2.3.3 Sea level index point models

As pointed by Ashe et al. (2019) in a compilation of statistical modeling methods for relative sea level, RSL models from SLIPs allow the study of sea-level changes for larger timescales than modern records. The authors mention that, as in the case of another type of sea-level information (e.g., Tide gauges, core records), the objective of statistical models is to estimate relative sea level evolution. That allows to quantify rate changes, identify spatial variability, and compare with other sources of sea-level information.

In their compilation, Ashe et al. (2019) identify five different statistical techniques used in the literature for sea-level index points (SLIPs).

1. Simple Linear Regression
2. Errors-in-variable Change-point
3. Errors-in-variable Integrated Gaussian process
4. Probabilistic Ensembles

2. Theoretical framework

5. Gaussian processes

In the compilation, Ashe et al. (2019) analyze the different methods from a hierarchical statistical modeling perspective. The authors identify two different levels for the hierarchical modeling of RSL with SLIPs: data and process level. In this context, the data level corresponds to the observation and measurement of the process (e.g., temporal uncertainties) and the process level to the characteristics of sea-level changes (e.g., variability, process noise).

These models have different approaches to handling SLIPs concerning their data and process levels. One main difference in the data level is how the temporal uncertainty of SLIPs is included. Ashe et al. (2019) point out that contrary to instrumental measurements of sea level, SLIPs inherit significant temporal uncertainties from dating techniques (i.e., radiometric dating). Some regression techniques assume time as an independent variable ignoring this aspect of SLIPs. Other methods such as Errors-in-variable techniques employ Markov chain Monte Carlo (MCMC) sampling distributions to include temporal uncertainties (Ashe et al., 2019).

2.4 Sea-level deterministic models

Sea-level changes combine the dynamics of various processes with different temporal and spatial extent (see Mitrovica and Milne, 2003; Shennan, 2015). One of the approaches to estimate the influence of these processes is the incorporation of modeling procedures. As pointed out by Ashe et al. (2019), Spatio-temporal sea-level models include a spectrum of approaches from purely statistical to purely physical models. Implementing purely physical (deterministic) models is typical for different sea-level processes. For example, to model global-to-regional processes as the glacial isostatic adjustment (GIA) (ΔISO_{GIA}), and local $\Delta LOCAL$ processes as changes due to the tidal regime and sediment compaction (see Shennan, 2015). For the temporal scope of the study, GIA models (ΔISO_{GIA}) are of interest for comparison with sea-level indicators. Milne (2015) points out that during the Quaternary, the glacial isostatic adjustment is the process that records the response to the main driver of relative sea level for this period: variations of spatial distribution and volume of ice sheets.

2.4.1 Glacial isostatic adjustment models

The objective of GIA models is to estimate the isostatic response of the earth to the redistribution of ice-water mass (see Milne, 2015; Shennan, 2015). Even though first

2. Theoretical framework

references to effects of ice-water mass distribution in sea-level changes are attributed to Jamieson (1865), Farrell and Clark (1976) first introduced physical modeling of this process. For the modeling of sea-level changes, Milne (2015) identifies two significant consequences of ice-water mass distribution: changes in the vertical position of the ocean floor and changes in the ocean surface. On the one hand, changes of the ocean floor (**R** Solid surface) result from isostatic deformation (i.e., elastic response). On the other hand, changes in the ocean level correspond to changes in the earth's gravitational field (due to mass redistribution) and the influx of water (e.g., meltwater) into the oceans.

Milne (2015) highlights the nature of these changes and their relevance for GIA models. For example, consequences due to the influx or outflow of water are considered eustatic changes (i.e., ΔEUS) and are not included in the GIA component. Similarly, the modeled GIA component is relevant to the isostatic effect (ΔISO), but it is not the only factor. The isostatic (ΔISO) component also includes the gravitational attraction effect responding to GIA. As explained by Rovere et al. (2016b), the mutual gravitational pull between water masses and ice sheets varies depending on the distribution and relative size of both elements. This component is called sea-level fingerprint ($\Delta ISO_{fingerprint}$). Consequently, GIA models require additional sea-level fingerprints modeling to represent all isostatic changes. In general, for areas without other isostatic phenomena (e.g., volcanic or karst isostasy), the following relation applies:

$$\Delta ISO = \Delta ISO_{GIA} + \Delta ISO_{fingerprint} \quad (2.11)$$

To estimate ΔISO_{GIA} , modelers integrate the different interactions between ice-water mass redistribution and relative sea level using different versions of the *sea-level equation* proposed by Farrell and Clark (1976). Beyond the mathematical particularities of the *sea-level equation* discussed by Farrell and Clark (1976), Milne (2015) illustrates the fundamental components of GIA modeling in relationship with this equation. First, the author identifies two inputs required to solve the sea-level equation: and Ice and Earth model. The former describes the Spatio-temporal evolution of ice sheets, and the latter the physical properties of the earth. Milne (2015) points out that both inputs derive from adopting paradigms that describe the structure and behavior of materials (e.g., rheological models) and their interactions. GIA modelers aim to find the set of conceptual models (e.g., lithospheric model), parameters (e.g., mantle viscosity), and variation of the *sea-level equation* that better describe observed sea-level changes.

2. Theoretical framework

Milne (2015) points out that GIA modelers modify the parameters to determine those that better adjust to other relative sea level information. Due to the increasing complexity of the input models, the addition of parameters, and variations to the *sea-level equation*, determining the best fitting model requires automated approaches. As an example relevant for this study, the GIA models used by Dendy et al. (2017) and Dyer et al. (2021) have three parameters related to the physical properties of earth and two parameters related to ice-sheets evolution. The former corresponds to the upper and lower mantle viscosity and the lithospheric thickness. Furthermore, the latter corresponds to the *Ice model* and the *ice propagation line*. For the earth's properties, parameters vary in physical values. For example, Upper mantle viscosity has two possible values (0.3 or $0.5 \times 10^{23} \text{ Pas}$), while the lower mantle has six different options (3 to $30 \times 10^{23} \text{ Pas}$ in irregular steps). In contrast, ice parameters often output from other modeling methodologies for a particular subprocess. For example, the *Ice model* parameter could take the values from ice thickness evolution from a series of models as the 'ICE6G' published by Roy and Peltier (2015).

3

Methodology

The proposed methodology for comparing sea-level indicators and sea-level models consists of algorithms to compute the difference between *RSL* recorded by SLIs and the glacial isostatic adjustment models ($\Delta ISO_{GIA}(\varphi, t)$). Due to their differences, SLI and limiting data points have different manipulations. In general terms, the methodology consists of random sampling in both age and RSL parameters for the SLI and then compute a Monte Carlo simulation process that randomly samples the GIA models and calculates the difference with SLI values. Following Equation (2.6) and (2.11) the subtraction results in a residual (ε):

$$\begin{aligned}\Delta RSL(\varphi, t) - \Delta ISO_{GIA}(\varphi, t) &= \Delta ISO_{fingerprint} + \Delta EUS(t) \\ &\quad + \Delta TECT(\varphi, t) + \Delta LOCAL(\varphi, t) + \Delta UNSP(\varphi, t)\end{aligned}\tag{3.1}$$

$$\varepsilon = \Delta RSL(\varphi, t) - \Delta ISO_{GIA}(\varphi, t)\tag{3.2}$$

$$\begin{aligned}\varepsilon &= \Delta EUS(t) + \Delta ISO_{fingerprint}(\varphi, t) + \Delta TECT(\varphi, t) \\ &\quad + \Delta LOCAL(\varphi, t) + \Delta UNSP(\varphi, t)\end{aligned}\tag{3.3}$$

3.1 Extraction of distribution parameters

As the database structure of WALIS proposed by Rovere et al. (2020) allows multiple chronological constraints for a single SLI, an initial step requires the extraction of the distribution parameters for Age and RSL. The following section explains the method to extract each component from the SLI.

3. Methodology

3.1.1 Sea level index points

Age

For the WALIS database structure (see Rovere et al., 2020), there are two types of age constraints: (1) radiometric dating (absolute dating) and (2) MIS Assignment (relative dating). In the latter, temporal constraints are considered continuous uniform distribution as it is equally probable that the SLI lies at any point within the time constraint range. Consequently, age parameters for uniform distributions are *Lower Age* and *Upper Age*. In contrast, radiometric dating ages are reported from their dating techniques as normal distributions. For that case, extraction parameters consist of the mean value (μ) and two times the standard deviation 2σ of the age estimation. After identifying and extracting the Age constraints parameters, each constraint (dating method) is assigned an equal probability to be the correct constraint. For example, for an SLI with N number of chronological constraints, every constraint is assigned the same probability parameter ($prob$) following the equation:

$$prob = 1/N \quad (3.4)$$

Table 3.1 shows the resulting extraction of Age parameters for sea-level indicator RSL_700 from Puglia, Italy (Cerrone et al., 2021). In this example, the SLI have more than one temporal constraint from different dating techniques (i.e., radiometric dating and MIS assignment).

Table 3.1: Extraction of Age parameters for SLIPs

Type of datapoint	Age calculation from	μ	2σ	Lower age	Upper age	Probability
Sea Level Indicator	Radiometric dating	139.6	4.5	NA	NA	0.17
Sea Level Indicator	Radiometric dating	138.0	14.0	NA	NA	0.17
Sea Level Indicator	Uniform distribution from MIS assignment	NA	NA	115	130	0.17
Sea Level Indicator	Uniform distribution from MIS assignment	NA	NA	94	104	0.17
Sea Level Indicator	Uniform distribution from MIS assignment	NA	NA	115	130	0.17
Sea Level Indicator	Uniform distribution from MIS assignment	NA	NA	71	130	0.17

Uniform distributions in peaks There is a variation in the extraction of Age parameters for uniform distributions. This variation allows the extraction from only the age ranges that correspond to peaks (highstand) of sea level in the stack published by Spratt and Lisiecki (2016) (Figure 3.1). This stack of sea-level variation during the last 800 ka comes from multiple proxies from ocean sediment core data. The peaks and their characteristics (e.g., width, initial, and endpoint) are determined using the `findpeaks()` functions from the `pracma` package (see Borchers, 2021).

3. Methodology

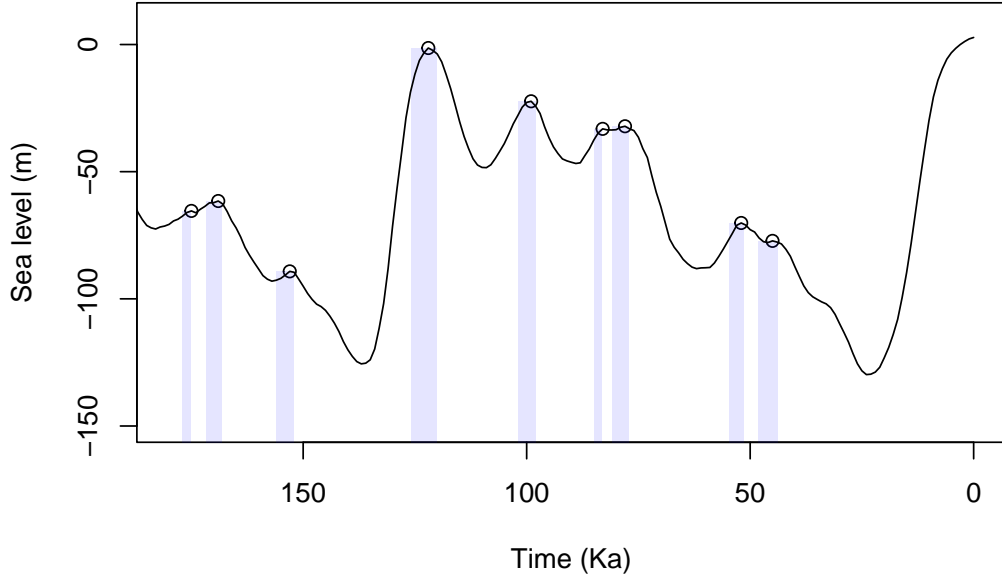


Figure 3.1: Ranges for uniform distribution sampling from sea level high stands. Blue areas correspond to age ranges to sample.

An age range from peaks is defined by the width W_{ap} of the range (Initial A_{Ip} and Endpoint of peak A_{Ep}), the age of peak maximum (A_{Mp}) and a factor (f) adjusting the width of the range. Given a peak with $A_{Ip} = 10$, $A_{Mp} = 20$, $A_{Ep} = 32$, and $f = 0.1$ the range limits is define as:

$$\begin{aligned} W_{ap} &= A_{Ep} - A_{Ip} \\ W_{ap} &= 32 - 10 \\ W_{ap} &= 22 \end{aligned} \tag{3.5}$$

$$\begin{aligned} [A_{Mp} - (W_{ap} * f), A_{Mp} + (W_{ap} * f)] \\ [20 - (22 * 0.1), 20 + (22 * 0.1)] \\ [17.8, 22.2] \end{aligned} \tag{3.6}$$

Code required to extract peaks from the sea-level stack published by Spratt and Lisiecki (2016) is available in the file `Methods\define_peaks_ranges.R`.

As a uniform constraint could intersect more than one peak range, one uniform distribution from the initial age constraints could result in different smaller uniform distributions around sea-level peaks. In that case, the *peak ranges* (Figure 3.1) replace the initial age constraints, and its probability *prob* corresponds to the division by the number of *peak ranges* intersected. Table 3.2 illustrates the parameter extraction for SLI RSL_700 in which one of the initial age constraints

3. Methodology

intersects multiple *peak ranges*. For Age constraints that do not intersect any *peak range*, extraction parameters stay unmodified. Similarly, temporal constraints from radiometric ages stay unmodified (parameters and *prob* value). Age extractions using this method are denominated as *Peak sampling* for future references in this text. An extraction of Age that keeps the original Uniform distribution parameters is called *No-peak sampling*.

Code required to extract the Age parameter from sea-level indicators is available in `Methods\extract_age.R`.

Table 3.2: Extraction of Age parameters for SLIPs with uniform sampling around sea level peaks.

Type of datapoint	Age calculation from	μ	2σ	Lower age	Upper age	Probability
Sea Level Indicator	Radiometric dating	139.6	4.5	NA	NA	0.17
Sea Level Indicator	Radiometric dating	138.0	14.0	NA	NA	0.17
Sea Level Indicator	Uniform distribution from MIS assignment	NA	NA	120.2	125.8	0.17
Sea Level Indicator	Uniform distribution from MIS assignment	NA	NA	98.0	102.0	0.17
Sea Level Indicator	Uniform distribution from MIS assignment	NA	NA	120.2	125.8	0.17
Sea Level Indicator	Uniform distribution from MIS assignment	NA	NA	77.1	80.9	0.04
Sea Level Indicator	Uniform distribution from MIS assignment	NA	NA	83.2	84.8	0.04
Sea Level Indicator	Uniform distribution from MIS assignment	NA	NA	98.0	102.0	0.04
Sea Level Indicator	Uniform distribution from MIS assignment	NA	NA	120.2	125.8	0.04

Relative sea level (RSL)

For the RSL, the parameter extraction follows the methodology explained by Garzón and Rovere (2021) to compute the percentiles of the RSL distribution. For RSL indicators of *Sea level indicator* or *Single Speleothem* type, the parameters correspond to a normal distribution with mean (μ) and standard deviation σ (see Equations (2.7) and (2.10)). For RSI indicators that are of *Single Coral* type, additional calculations and parameters are required as RSL is assumed to have a gamma distribution. First, the parameters α and β from the gamma distribution result from interpolation using the *Upper limit of living range* and *Lower limit of living range* parameters as the 2.3 and 97.7 percentiles. Second, the elevation E parameters are extracted from the *Elevation* and *Elevation error* parameters from the WALIS database. Similar to the Age extraction, every constraint is assigned the same probability (*prob*) parameter (see Equation (3.4)).

Table 3.3: Extraction of RSL parameters for single corals indicators

Type of datapoint	RSL Indicator	Upper limit U_1 (m)	Upper limit L_1 (m)	Elevation (m)	Elevation error (m)	α	β	Probability
Sea Level Indicator	Single Coral	-3	-10	3.5	0.5	11.48	1.92	1

Table 3.3 shows the resulting extraction of RSL parameters for *Single Coral*

3. Methodology

indicator RSL_700.

Table 3.4: Extraction of RSL parameters for sea-level indicators

Type of datapoint	RSL Indicator	Paleo RSL μ	Palo RSL uncertainty σ	Probability
Sea Level Indicator	Marine Terrace	28.9	5.84	0.17
Sea Level Indicator	Marine Terrace	28.9	5.84	0.17
Sea Level Indicator	Marine Terrace	28.9	5.84	0.17
Sea Level Indicator	Marine Terrace	28.9	5.84	0.17
Sea Level Indicator	Marine Terrace	28.9	5.84	0.17
Sea Level Indicator	Marine Terrace	28.9	5.84	0.17

Table 3.4 shows parameter extraction for the sea-level indicator USeries_52 from Crawl Key (Chutcharavan and Dutton, 2021). All parameters for the different constraints are identical as sea-level indicators RSL usually come from a single observation (e.g., A single *Indicative range*). Code required to extract the *RSL* parameter from sea-level indicators (SLIs) is available in the file `Methods\extract_RSL.R`.

3.1.2 Limiting data

Age

For limiting data (marine and terrestrial limiting), extraction of the Age parameter follows the same methodology as sea-level index points (SLIPs) described before.

Relative sea level (RSL)

For RSL, the parameter extraction identifies the indicator type (i.e., marine and terrestrial) and defines its limiting level and uncertainty of the measurement.

Table 3.5: Extraction of RSL parameters for limiting indicators

Type of datapoint	RSL Indicator	Paleo RSL μ	Palo RSL uncertainty σ
Terrestrial Limiting	The datapoint is a marine or terrestrial limiting indicator	-5.65	1.18
Terrestrial Limiting	The datapoint is a marine or terrestrial limiting indicator	-5.65	1.18
Terrestrial Limiting	The datapoint is a marine or terrestrial limiting indicator	-5.65	1.18

Table 3.5 shows parameter extraction for sea-level indicator RSL_3764 from West Sussex, Great Britain (UK)(Cohen et al., 2021). As in the previous case, all RLS parameters are equal.

3. Methodology

3.2 Merging sea-level indicators

After extraction of Age and RSL parameters, all constraints of individual sea-level indicators (SLI) are merged into a single Age and RSL constraint. The merging method and output type vary depending on the *Type of datapoint* (i.e., SLIP or limiting) of each SLI.

3.2.1 Sea level index points merge

For both Age and RSL, the sea-level index points (SLIPs) merging results from applying a Monte Carlo sampling technique. This sampling strategy is a variation of the method proposed by Bender et al. (2020). The sampling consists of two steps: randomly select a constraint (see Table 3.2 for Age and 3.4 for RSL) and then randomly select a value using its Age/RSL distribution parameters. For RSL in *Single Coral* samples, the value selection requires sampling from the *living range* gamma distribution (Upper and lower) and the normal distribution of the elevation to compute the RSL. The sum of both values results in the RSL of the sea-level indicator. This calculation is not required for other types of indicators as RSL is already available by applying Equations (2.7) to (2.10). This process is repeated P times (defined by the user) and results in a point cloud of RSL and Age values.

Figure 3.2 illustrates the differences in *Age* and *RSL* distributions between the same SLIP by applying the *No-peak sampling* and the *Peak sampling* method.

3.2.2 Limiting indicators merge

For limiting indicators, Age and RLS parameters have different merging strategies.

For Age, limiting indicators with only one temporal constraint are not sampled as SLIPs, but they inherit the original distribution parameters. In contrast, limiting indicators with more than one temporal constraint follow the same sampling procedure for SLIPs. For RSL, the merged constraint corresponds to the most informative limiting indicator. Figure 3.3 illustrates the most informative indicator selection from a group of only terrestrial or marine limiting indicators. There is no implementation for merging opposite indicators (e.g., one terrestrial and one marine limiting) as the WALIS database does not include examples of such a combination of limiting indicators.

3. Methodology

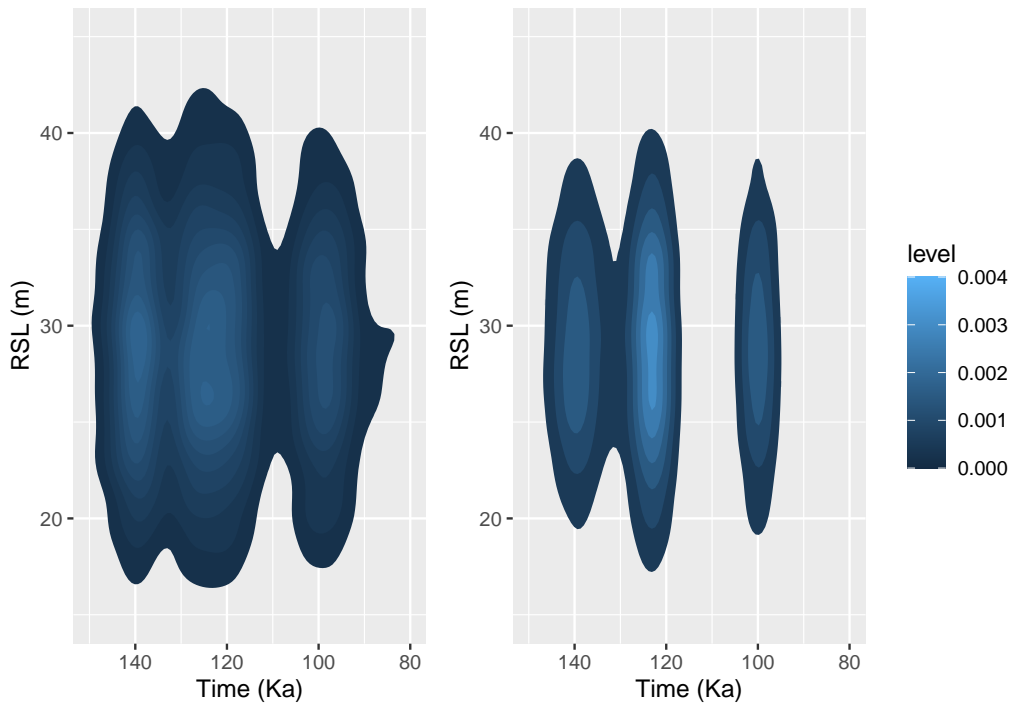


Figure 3.2: SLI sampling with two different Age sampling strategies. (Left) No-peak sampling (Right) Peak-sampling.

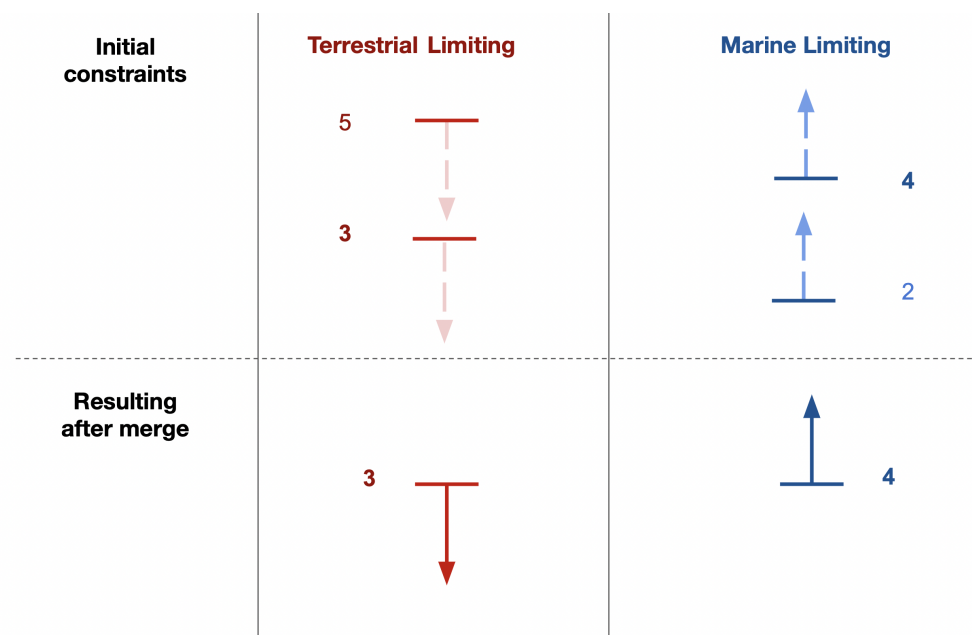


Figure 3.3: Merging of terrestrial and marine limiting data. The most informative indicator for each group is selected.

3. Methodology

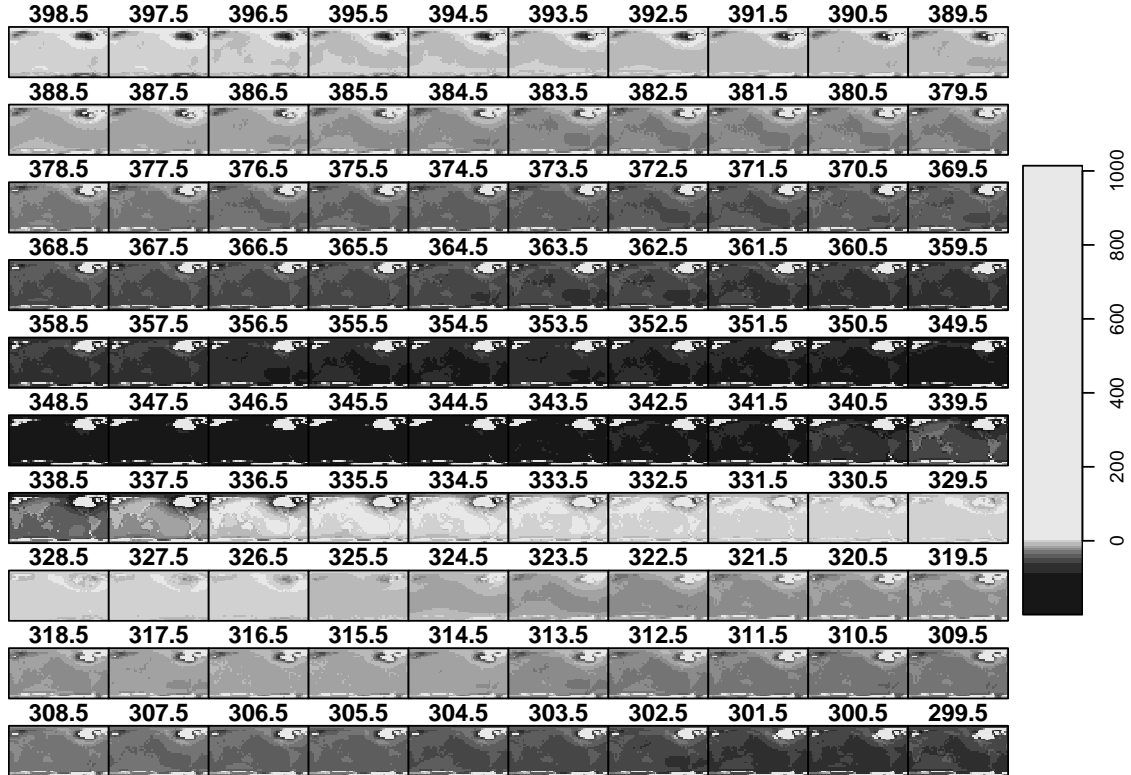


Figure 3.4: GIA model portion for one parameter configuration. Lithospheric thickness=48 km, Upper mantle viscosity=0.3 10e23 Pa S, Lower mantle viscosity=3 10e23 Pa S, Ice model= Colleoni model, Propagation line = Wael-S.

3.3 GIA models as a data cube

The GIA models selected to compare with the sea-level indicators are a portion of 216 models that partially correspond to the models used by Dendy et al. (2017) and Dyer et al. (2021). Each model corresponds to a different configuration of Ice and Earth modeling parameters and covers the last 400 ka. The authors shared the models as two hundred sixteen (216) .mat files (®Matlab). The name of each file stores the five parameter configuration of each model. Two hundred sixteen files were transformed into a single NetCDF file as an 8-dimensional data cube to simplify the operations and interaction with the collection of models. The models result in a 256x512 (lat-long) spatial grid with relative sea level (RSL) values from the GIA component (ISO_{GIA}). Each model has 599 layers corresponding to a particular time from 400 to 0 ka. Table 3.6 summarizes the dimensions and characteristics. Figure 3.4 corresponds to a portion of the GIA model output for a specific parameter configuration.

3. Methodology

Table 3.6: GIA models parameters

Dimension	Number of parameters	Values	Units	Interval
Time	599	0 to 400	ka	irregular
Longitude	512	0 to 359.29	degrees	0.703125
Latitude	256	89.46 to -89.46	degrees	irregular
Lithospheric thickness	3	48 to 96	km	irregular
Upper mantle viscosity	2	0.3 to 0.5	10e21 Pa s	0.2
Lower mantle viscosity	6	3 to 30	10e21 Pa s	irregular
Ice Model	3	Colleoni\ICE6G\Lambeck	Model type	-
Propagation	2	Wael-s & Wael-T	Propagation model type	-

3.4 Residual calculation

To compute the residual (ε) value (see Equation (3.1)), it is required to extract all SLIPs and GIA models from a selected area. As a first step, all sea-level indicators (i.e., Sea level index points and limiting indicators) are individually merged. After the merging and parameter extraction, only sea-level index points (SLIPs) are selected for sampling. Limiting indicators are omitted as unbounded RSL intervals complicate their integration. Second, from the selection of SLIPs, the *Age* and *RSL* values are sampled using their distribution parameters. All SLIPs are sampled by an equal number of points (usually 10.000), and their values are grouped into a single collection (point cloud). Each feature includes the WALIS_ID of origin, associating the random selection with a specific indicator. Third, the Age and RSL values ($\Delta RSL(\varphi, t)$) are sampled by a proportion of the point cloud size (e.g., 10% or 30%) and compared applying Equation (3.2) with a random selection of one of the 216 GIA models. GIA models values are selected from the closest location to the SLI indicators. That means that each point is compared using a random model from the collection of nearest GIA models. As the *Age* parameter of the point clouds does not necessarily match the *Age* parameter of GIA Models (0 to 400 Ka with 0.5 and 1.0 Ka spacing), values are linearly interpolated from the nearest lower and upper value. Figure 3.5 illustrates the sampling process for collecting Age and RSL 100.000 values with a GIA sampling proportion of 10%.

Code required to compare sea-level index points (SLIPs) cloud points and GIA models is available in the file `Methods\compare_sli_gia.R`.

3.5 Curve fitting

Values resulting from the residual calculation are distributed irregularly along the age dimension depending on the distribution of ages of SLIPs. That results in gaps

3. Methodology

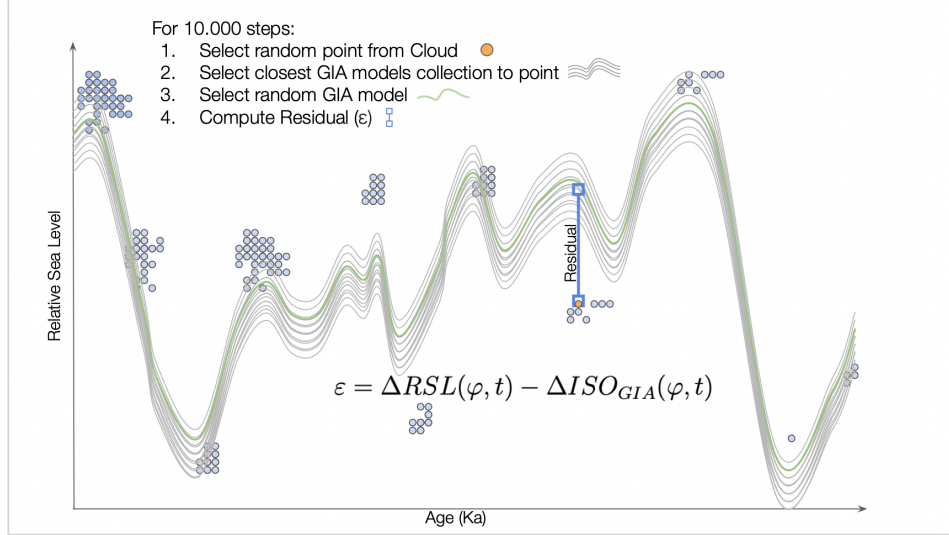


Figure 3.5: Computation of Residual from SLI and GIA models

on the temporal dimension with none to little age values (outliers). The residual curve is fitted by parts to avoid using values from low-density temporal ranges. Regions of importance (high density) are identified using the kernel density estimate. Values in age ranges with less than 15% of the maximum relative density value are excluded for the fitting. Lastly, residual values in the high-density age ranges are fitted individually using a generalized additive model (GAM).

3.6 Evaluation - Case studies

Two areas with different geological characteristics were selected to test the methodology. The selected areas are: 1) the passive tectonic margin from the South American Atlantic coast and 2) the active tectonic margin from the Pacific coast. Each area was divided into four sub-regions to test whether the methodology differentiates regional trends by mean residual values. SLIPs in the area were extracted from the World Atlas of Last Interglacial Shorelines database (WALIS) using the location parameter. Table 3.7 shows the WALIS compiler and SLIPs references by case study. The areas were compared with the *No-peak sampling* and *Peak sampling* methods for uniform age constraints to test the differences due to the extraction method (i.e., sampling method). Each sea-level index point was sampled 10.000 times for RSL and Age values. For example, a sub-region with 100 SLIPs would result in an RSL/Age point cloud of 1.000.000 values. Subsequently, 30% of the RSL/Age point cloud from the regions was compared with the GIA values from the area to obtain the residual (ε) value. The identification of SLIPs (i.e., WALIS ID)

3. Methodology

of origin and model parameters from the GIA value is included to test potential residual differences due to these parameters.

Given the characteristics of the proposed methodology and the resulting residual values, evaluating differences in the central tendency by model parameters would require additional modeling of the process. As an alternative, in the case studies, differences in central tendency by grouping parameters (e.g., model parameters, region, specific model) are evaluated using the non-parametric statistical Kruskal-Wallis and Wilcoxon test. However, results from these tests must be held with caution as residual values do not meet the assumption of independence.

Code required to compare Residual (ε) from different regions is available in the file `Methods\compare_regions.R`.

3.7 Methodology reproducibility

This document is machine-generated using the `Oxforddown` thesis template published by Lyngs (2019). The code required to reproduce all sections of this document is available at https://github.com/SbastianGarzon/sea_level_indicators_and_models. The repository contains three main folders, `Methods`, `Dissertation` and `Data`. In the `Methods` folder, there are the R scripts required to perform the different steps of the proposed methodology. The `Dissertation` folder contains Rmarkdown files for the different chapters of this document (e.g., `Dissertation/03-methodology.RMD` corresponds to this chapter). Consequently, all figures and tables (except diagrams) in this document are reproducible. After installing the required libraries (see. `renv.lock` file), knit the `index.Rmd` file to generate the document. The `Data` folder contains the required external data sets that correspond to the WALIS summary table (`walis.csv`) (see Rovere et al., 2020), the collection of GIA models (`GIA_Austermann_2019.nc`) (see Dendy et al., 2017; Dyer et al., 2021), the sea-level stack published by Spratt and Lisiecki (2016) and the delimitation of the areas for the case studies (`CaseStudy_1.kml` and `CaseStudy_1.kml`). The Github repository does not contain the GIA models file (60GB) (see Dendy et al., 2017; Dyer et al., 2021) as these models were privately shared for this project by the authors. Request to access the GIA data sets can be sent to jgarzon@uni-muenster.de.

3. Methodology

Table 3.7: WALIS References by case study

WALIS Compilator	References
South America - Atlantic	
Rubio-Sandoval et al. (2021)	Martins et al. (2018), Filho and Olmiro (2017), Suguió et al. (2011), Horn Filho and Simó (2008), Tomazelli and Dillenburg (2007), Tomazelli et al. (2006), Suguió et al. (2003), Barreto et al. (2002), Bujalesky et al. (2001), Dominguez et al. (1990), Martin et al. (1988), Poeupeau et al. (1988), Barbosa et al. (1986), Suguió et al. (1985), Villwock (1984), Bernat et al. (1983), Martin (1982), Suguió et al. (1982), Bittencourt et al. (1979), Martin et al. (1979), Martin and Suguió (1976), Suguió and Petri (1973)
Gowan et al. (2021)	Björck et al. (2021), Pappalardo et al. (2015), Isla and Angulo (2015), Gordillo and Isla (2011), Fucks et al. (2010), Gordillo et al. (2010), Rabassa et al. (2008), Bujalesky (2007), Bujalesky and Isla (2006), Fucks et al. (2006), Isla et al. (2000), Rostami et al. (2000), Schellmann and Radtke (2000), Schellmann and Radtke (1999), Schellmann (1998), Schellmann and Radtke (1997), Aguirre et al. (1995), Aguirre and Whatley (1995), Rutter et al. (1990), Radtke (1989), Rutter et al. (1989), Albero and Angiolini (1983), Codignotto (1983), Bayarsky and Codignotto (1982)
South America - Pacific	
Freisleben et al. (2021)	Martinod et al. (2016), Jara-Muñoz et al. (2015), Saillard et al. (2012), Victor et al. (2011), Saillard et al. (2011), Pfeiffer et al. (2011), Regard et al. (2010), Saillard et al. (2009), Pedoja et al. (2009), Melnick et al. (2009), Saillard (2008), Quezada et al. (2007), Pedoja et al. (2006a), Pedoja et al. (2006b), Villalobos and Pino (2005), Dumont et al. (2005), Marquardt et al. (2004), Pedoja (2003), González et al. (2003), Pino et al. (2002), Zazo (1999), Vargas and Ortíeb (1998), Schellmann and Radtke (1997), Ortíeb et al. (1996), Hartley and Jolley (1995), Ota et al. (1995), Ortíeb et al. (1995), Macharé and Ortíeb (1994), Iriondo (1994), Macharé and Ortíeb (1992), Leonard and Wehmiller (1992), Hsu (1992), Goy et al. (1992), Paskoff (1991), Leonard and Wehmiller (1991), Ortíeb et al. (1991), Ortíeb and Macharé (1990), Radtke (1989), Hsu et al. (1989), Radtke (1987), Paskoff (1977)
Thompson and Creveling (2021)	Creveling et al. (2017)

4

Results

4.1 South American Atlantic coast (5-55° S)

4.1.1 Area of study

The South American Atlantic coast (see Figure 4.1) was divided into four different regions to compare sea-level indicators and GIA models using the proposed methodology in a passive margin. These areas correspond to the North East (BR[NE]) and South of Brazil (BR[S]), the Northern Argentinian and Uruguayan coast (ARG[NE]-UY), and the southeast of Argentina (ARG[SE]). There are a total number of 67 sea-level index points in the whole area of study. The selected sea-level index points are part of two SLIs compilations for the South American Atlantic coast published by Rubio-Sandoval et al. (2021) and Gowan et al. (2021) using the WALIS database standard. This compilation includes observations, measurements, and interpretations from 46 different publications in five different languages (English, Portuguese, Spanish, French, and German) since 1973 in this region. The criteria used to define the areas correspond to proximity (latitudinal distance) between sea-level indicators. Table 4.1 shows the total number of SLIPs and the origin of their age calculation (i.e., radiometric dating or MIS assignment).

4. Results

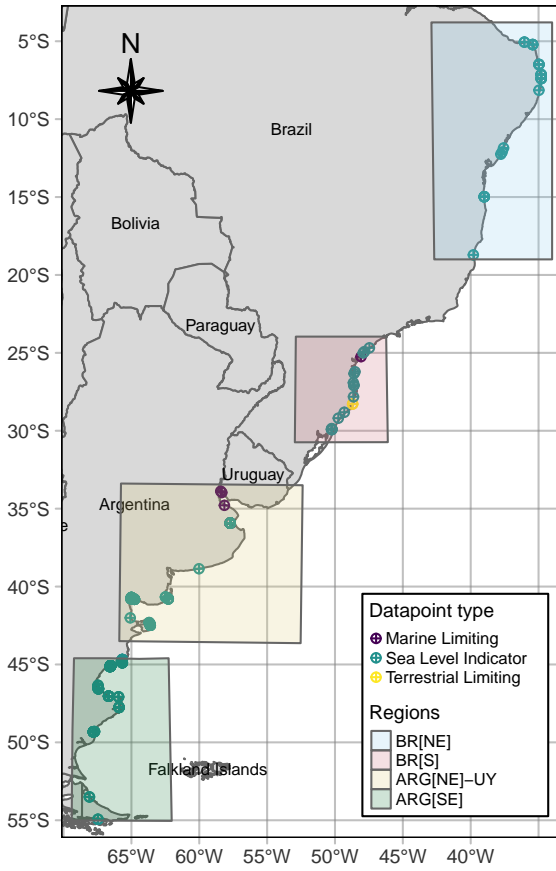


Figure 4.1: South American Atlantic coast. Regions and sea-level indicators location.

Table 4.1: South America Atlantic coast - Number of SLIPs by subregion

Region name	Number of sea level index points	Origin age calculation (Number of constraints)	
		Radiometric dating	MIS assignment (Uniform)
BR[NE]	11	22	5
BR[S]	16	0	16
ARG[NE]-UY	13	39	38
ARG[SE]	27	81	49

4.1.2 SLIPs Point cloud and GIA model values

Before comparing SLIPs and GIA models, the individual elements were extracted for each region. Figure 4.2 shows SLIPs after extraction (sampling) as clouds of points grouped by area (horizontal) from north to south and type of sampling (*No-peak sampling* and *Peak sampling*). Differences between the sampling techniques are evident in the Brazilian (South) region. In this area, the SLIPs point cloud locates around particular age ranges. This effect of the sampling method is also visible in the other areas with different intensities. The average value (lines) and

4. Results

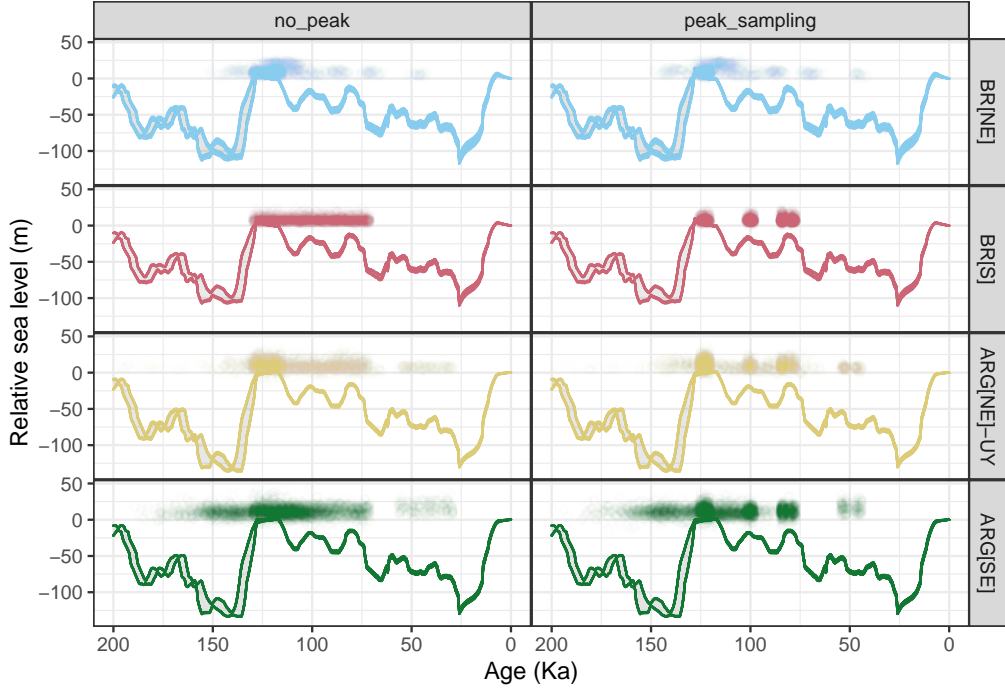


Figure 4.2: South American Atlantic coast SLIPs and GIA. Lines correspond to GIA models and points (Point cloud) to sea-level indicators resulting from SLIP sampling.

standard deviation (shaded area) of each of the 216 GIA model configurations by region are included in the graph (lines). The models show similar patterns during the last 200 ka for the four areas. For example, the models exhibit relatively high variation between 200 and 130 ka compared to the 130 to 0 ka period. As the main difference, the areas located in Argentina and Uruguay (ARG[NE]-UY - ARG[SE]) have lower relative sea level values between 160 and 130 ka than the Brazilian areas (BR[NE] and BR[S]).

4.1.3 Residual values

Comparison between SLIPs (Point cloud) and GIA models resulted in residual values for these regions. Figure 4.3 shows the fitted curves of residual values in high-density temporal ranges (i.e., more than 15% of highest age density) by area and sampling method. As the main difference between the sampling methods, residuals from *peak sampling* for uniform age distributions result in temporal ranges where no calculation of residual value is possible (i.e., no data). However, the residual levels and tendencies are similar for age ranges where both techniques have information. Both sampling methods on the Brazilian northeast coast (BR[NE]) result in a rapid increase of residual values from 125 to 110 ka. For Brazil (South) and Argentina (North)/Uruguay areas, residual values around 125 ka are lower (around 0-15m)

4. Results

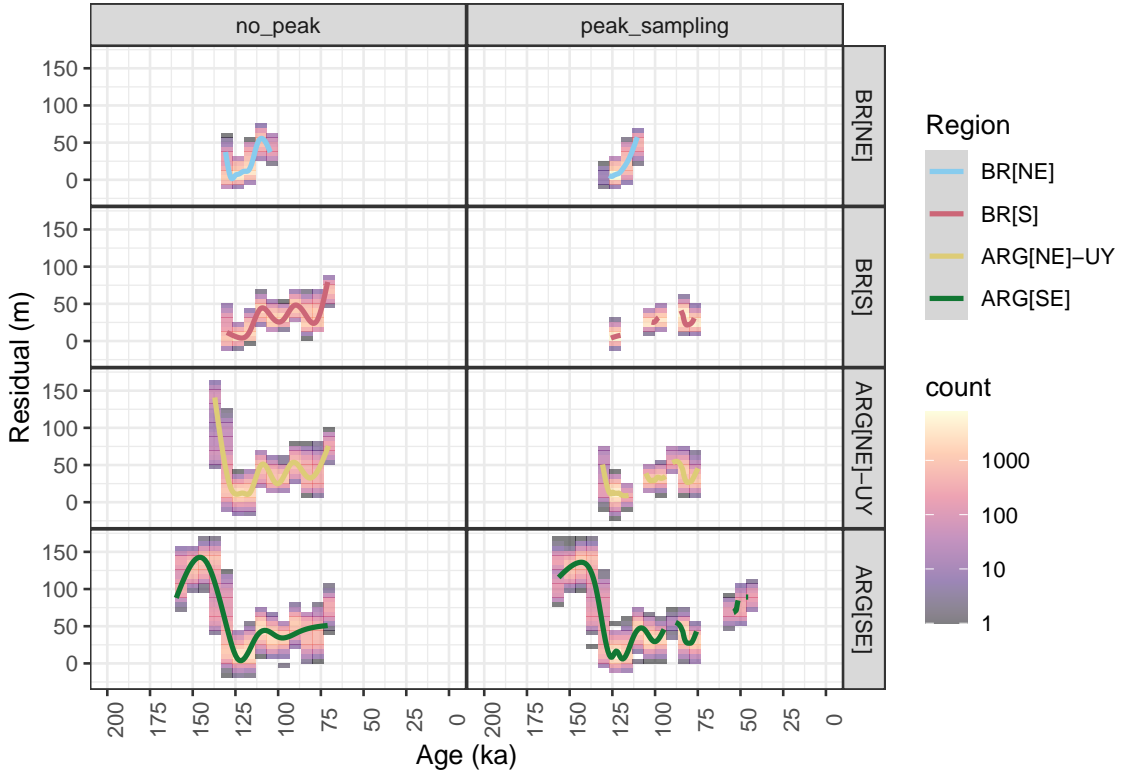


Figure 4.3: South American Atlantic coast. Residual values by region and sampling method. Solid line correspond to fitted line. Bins represent number of points (point cloud) by age and residual value.

than the levels at 100 and 80 ka (25-30m). The southeast Argentinian area is the only area with residual values (high density) before 140 ka. This area shows an initial residual increase (up to 150 m around 160 to 150 ka) and a posterior decrease to 0 m (around 125 ka). Similarly, this area is the only one that shows information (*peak sampling*) for the period around 50 ka with high residual levels between 60 and 90 m. From 125 to 75 ka, residual values from the Atlantic coast sub-regions fluctuate between 0 to 50 m.

4.1.4 Evaluation

Residual values partially result from the random selection of GIA models that have a particular configuration of parameters. For that reason, the comparison of residual values by their grouping parameters (e.g., lower mantle viscosity) could provide indications of residual values differences due to GIA models parameters. Figure 4.4 shows the mean residual values by model parameters (A to E) and by sampling method (F). Comparison between different grouping parameters (A to E) using the same sampling methods shows a similar distribution of mean values.

4. Results

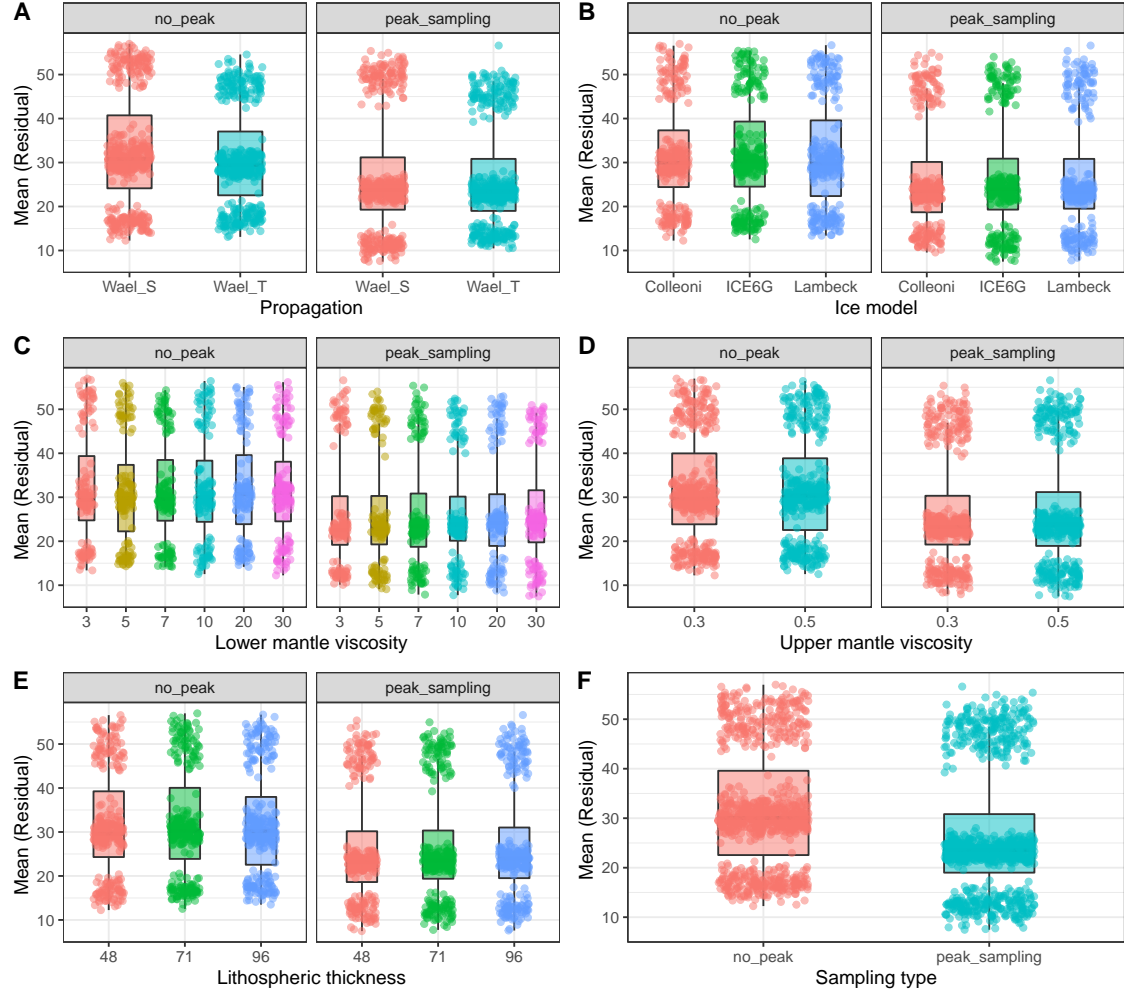


Figure 4.4: South American Atlantic coast mean residual values by model parameters and sampling method.

However, the residual values form three distinct groups that do not correspond to differences in the model parameters. As a general observation, residual values tend to be higher for residuals using *no-peak sampling* for all the model parameters (see Figure 4.4.F). This observation is supported by the Kruskal test result that rejects the H_0 hypothesis that the central tendency between sampling techniques is equal.

Additional Kruskal tests were applied to identify if differences in the central tendency of the residual values between different groups result from different GIA model parameters (see Table 4.2). The H_0 hypothesis for all tests is that the central tendency of all parameters is the same. Table 4.2 shows that for the *No-peak sampling*, almost all model parameters (except Propagation), region, and specific model (5 GIA model parameter combination), result in a P-value lower than 0.05 rejecting H_0 (P-values lower than 0.05 in **bold**). Similarly, for the cases using the *Peak sampling* method, H_0 is rejected for most model parameters (except Upper

4. Results

mantle viscosity), region, and specific model.

Table 4.2: South America Atlantic coast - Kruskal test

Parameter	Degrees of freedom	No peak sampling		Peak sampling	
		$\tilde{\chi}^2$	P-value	$\tilde{\chi}^2$	P-value
Region	3	23822.1	P<0.001	34814.0	P<0.001
Propagation	1	94.2	P<0.001	0.4	0.543
Ice	2	8.0	0.0185	6.1	0.0465
Lower mantle viscosity	5	22.9	P<0.001	43.4	P<0.001
Upper mantle viscosity	1	2.5	0.112	16.9	P<0.001
Lithospheric thickness	2	14.9	P<0.001	34.9	P<0.001
Model	215	396.3	P<0.001	362.9	P<0.001

A pair-wise Wilcoxon test was performed to determine the parameters configuration with different central tendencies for the residual values following the indications from the Kruskal test results that they differ by parameters, region, and specific models. Table 4.3 shows total possible combinations (Pairs) for each grouping parameter. For example, as Propagation only have two parameters (i.e., $Wael_S$ and $Wael_T$), there is only one possible pair. Table 4.3 shows how many of those pairs have statistically significant differences (P-value < 0.05) in their central tendency according to the Wilcoxon test. As a main result, all pairs of regions have statistically significant differences for both sampling techniques. For the *No-peak sampling*, the lower-mantle viscosity, Upper-mantle viscosity, and Lithospheric thickness grouping parameters also have pairs of values that are significantly different. Different results are obtained for the *Peak sampling* method, where only the Propagation and Lithospheric thickness parameters have consistent differences by residual values (i.e., a high proportion of significant different pairs) (see Table 4.3). Similarly, from the 23.220 possible pairs of models, only 7 and 1 have statistically significant differences in their central tendency for the *No-peak sampling* and *Peak sampling* methods.

Table 4.3: South America Atlantic coast - Pairwise Wilcoxon test

Grouping parameter	Number of pairs	No peak sampling		Peak sampling	
		Significant different pairs	Significant different pairs	Significant different pairs	Significant different pairs
Region	6		6		6
Propagation	1		0		1
Ice	3		0		1
Lower mantle viscosity	15		7		2
Upper mantle viscosity	1		1		0
Lithospheric thickness	3		3		2
Model	23220		7		1

4. Results

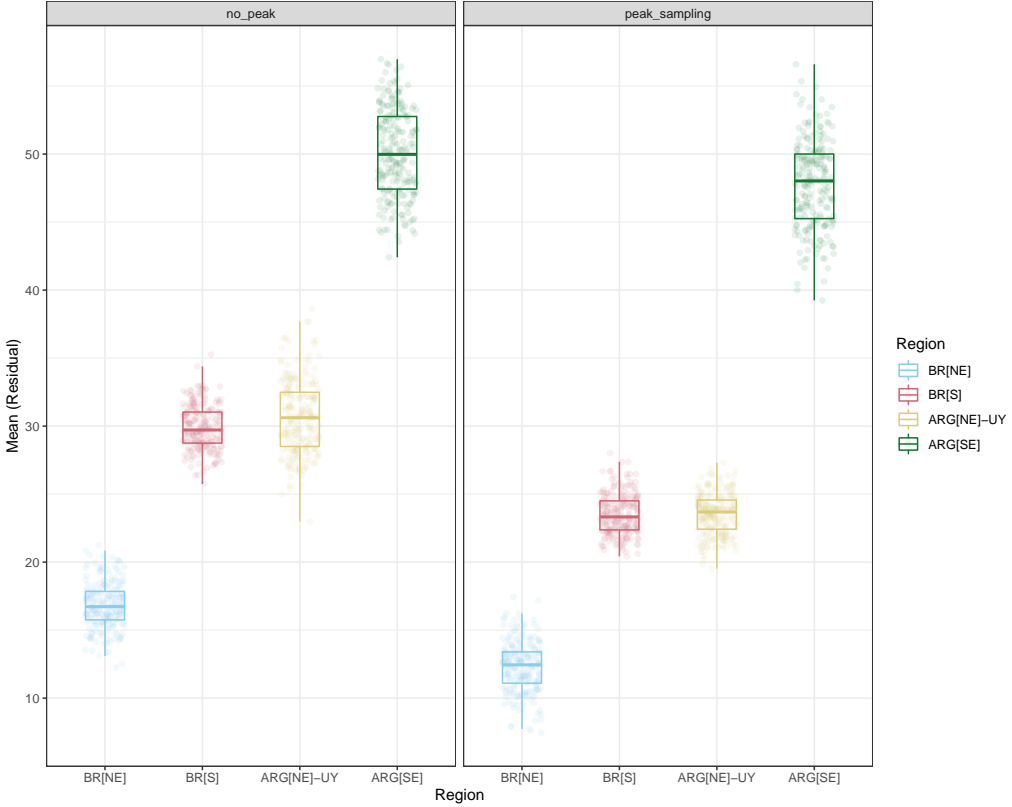


Figure 4.5: South American Atlantic coast mean residual values by region.

Mean residual values grouped by region are shown in Figure 4.5. The Kruskal tests suggest that the residual central tendency between different sampling techniques is different, showing lower mean values for the *Peak sampling* method if grouped by regions. Both sampling techniques show similar trends concerning the relative order between sub-regions. From north to south, the Brazilian northeast coast (BR[NE]) shows the smallest residual values, followed by the Brazilian south coast (BR[S]), the Argentinian (North-East)/Uruguay (ARG[NE]-UY), and the Argentinian southeast (ARG[SE]) with higher mean residual values.

4.2 South American Pacific coast (1°N-40°S)

4.2.1 Area of study

The proposed comparison methodology was tested in an active tectonic margin along four different regions in the pacific coast of South American (see Figure 4.6). These areas correspond to the Ecuadorian and northern Peruvian coast (Ecuador-Peru[n]), the central and southern Peruvian coast (Peru[C-S]), the northern and central Chilean coast (Chile[N] and Chile[C]). There are 1953 sea-level index points (type of

4. Results

data point) for the whole area of study. The selected sea-level index points include indicators included in the recompilation of Freisleben et al. (2021) and Thompson and Creveling (2021) using the WALIS database standard. This compilation includes observations, measurements, and interpretations from 43 different publications in three different languages (English, Spanish and French) since 1977 in this region. More than 80% of Age parameters in this region have a designated MIS uniform temporal constraint (see Table 4.4). The selected areas division corresponds to the four sectors proposed by Freisleben et al. (2021) based on the main geomorphic characteristics of the Pacific coast of South America.

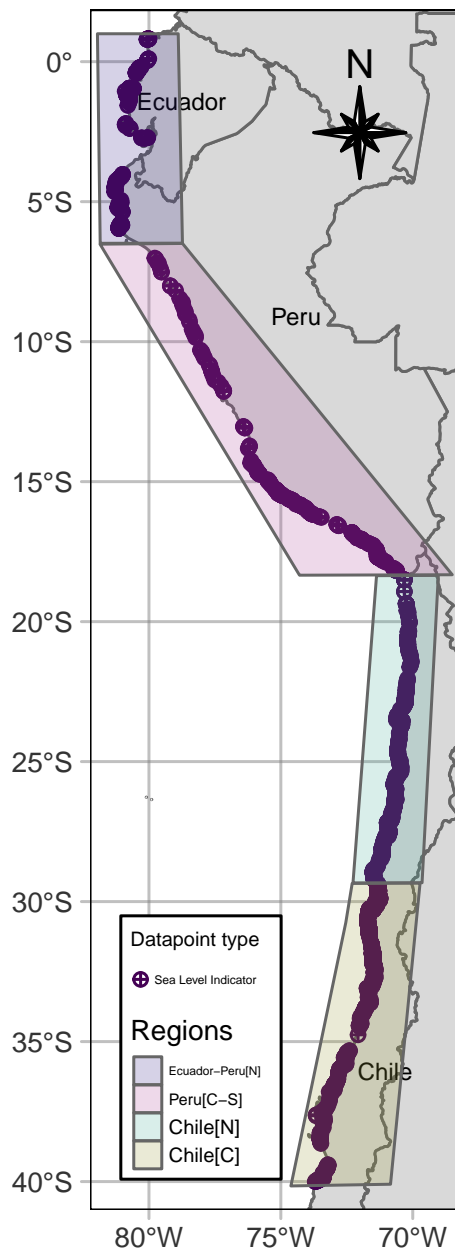


Figure 4.6: South American Pacific coast.

4. Results

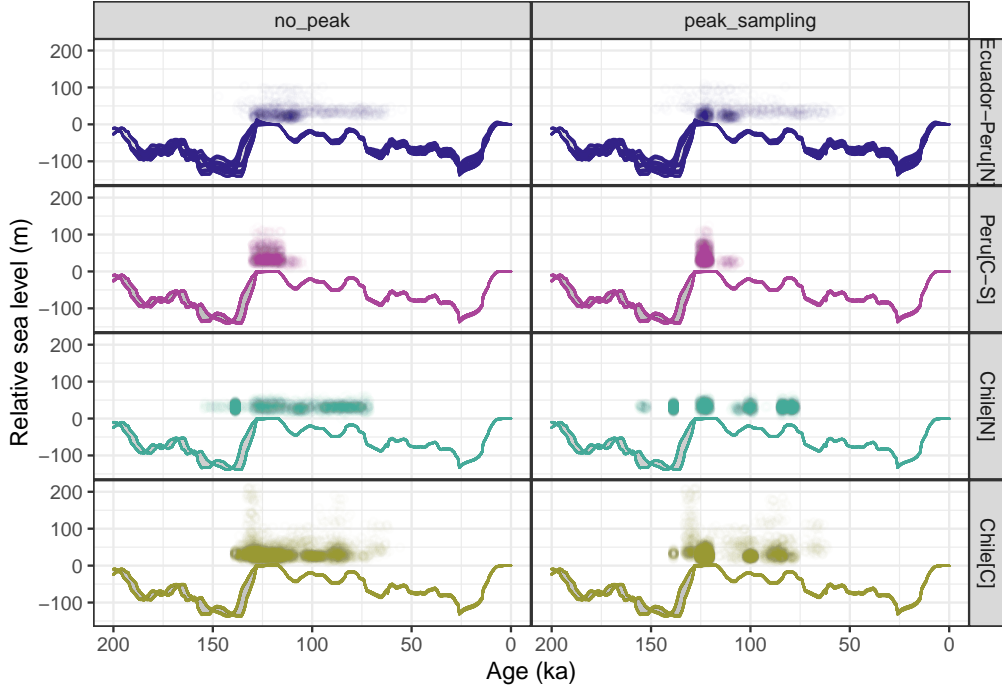


Figure 4.7: South American Pacific coast SLIPs and GIA. Lines correspond to GIA models and points (Point cloud) to sea-level indicators resulting from SLIP sampling.

Table 4.4: South America Pacific coast - Number of SLIPs by subregion

Region name	Number of sea level index points	Origin age calculation (Number of constraints)	
		Radiometric dating	MIS assignment (Uniform)
Ecuador-Peru[N]	205	162	94
Peru[C-S]	264	24	288
Chile[N]	545	25	523
Chile[C]	939	197	837

4.2.2 SLIPs Point cloud and GIA model values

Figure 4.7 shows the extraction of GIA models values (Lines) and SLIPs sampling (Point cloud) previous to the comparison. As for the South American Atlantic coast, GIA models in the Pacific coast have a similar trend with high variability of relative sea level between 200 and 130 ka and low variability between 130 and 0 ka. However, the Ecuadorian and northern Peruvian regions (Ecuador-Peru[N]) show higher variability in the 130 to 0 ka period. Point clouds of SLIPs show differences in the temporal extent of the information between groups. In specific, the Peruvian central and south areas (Peru [C-S]) only have residual values between 130 and 110 ka, while other regions cover more extended periods (e.g., Chile[N] covers from 160 ka to 75 ka). Due to the sampling methods, differences in the

4. Results

SLIPs cloud points are noticeable in all regions. For example, the *Peak sampling* for the northern Chilean area (Chile[N]) shows up to seven clearly defined Point cloud clusters, while the *No-peak sampling* method results in a more extended Point cloud. Regarding SLIPs relative sea level values, the central Chilean region (Chile[C]) shows values up to 200 meters for some periods while other regions' maximum values range between 60 and 110 m.

4.2.3 Residual values

The proposed comparison methodology between SLIPs and GIA models resulted in residual values for the South American Pacific coast. Figure 4.8 shows the fitted residual curves in high-density temporal ranges. As for the Atlantic coast, the difference in the sampling methods results in temporal ranges where no comparison is possible. This means that there are periods with no residual values to analyze. However, for the periods where both sampling techniques have residual values, all regions show similar trends for the *No-peak sampling* and *Peak sampling*. On the Ecuadorian and north Peruvian coast (Ecuador-Peru[N]), both sampling methods result in residual values of around 25 and 40 m at 125 ka, increasing to 80 m at 110 ka. The Peruvian central and south coast (Peru[C-S]) shows a residual level of approximately 50 m at 125 ka. Both the northern Chilean (Chile[N]) and central (Chile[C]) coast show higher residual values up to 170 m at 140 ka, with a posterior descent to 40 m around 125 ka. Similarly, both regions show residual levels around 50 m at 100 ka and 60 m around 80 ka. In general, from 125 to 75 ka residual values from the Pacific coast sub-regions fluctuate between 30 to 100 m which is a higher range than the Atlantic coast values (i.e., 0 to 50 m).

4.2.4 Evaluation

Figure 4.9 shows the mean residual values by model parameters (A to E) and by sampling method (F). Comparison between different grouping parameters (A to E) using the same sampling methods shows a similar distribution of mean values except for the Propagation parameter, where the difference is notable. As for the Atlantic coast, residual values tend to be higher for residuals using *No-peak sampling* for all the model parameters (see Figure 4.4). A Kruskal test with a P-value lower than 0.05 testing the H_0 hypothesis shows that there are differences in the central tendency values between sampling techniques.

Additional Kruskal tests were applied to identify differences in mean residual

4. Results

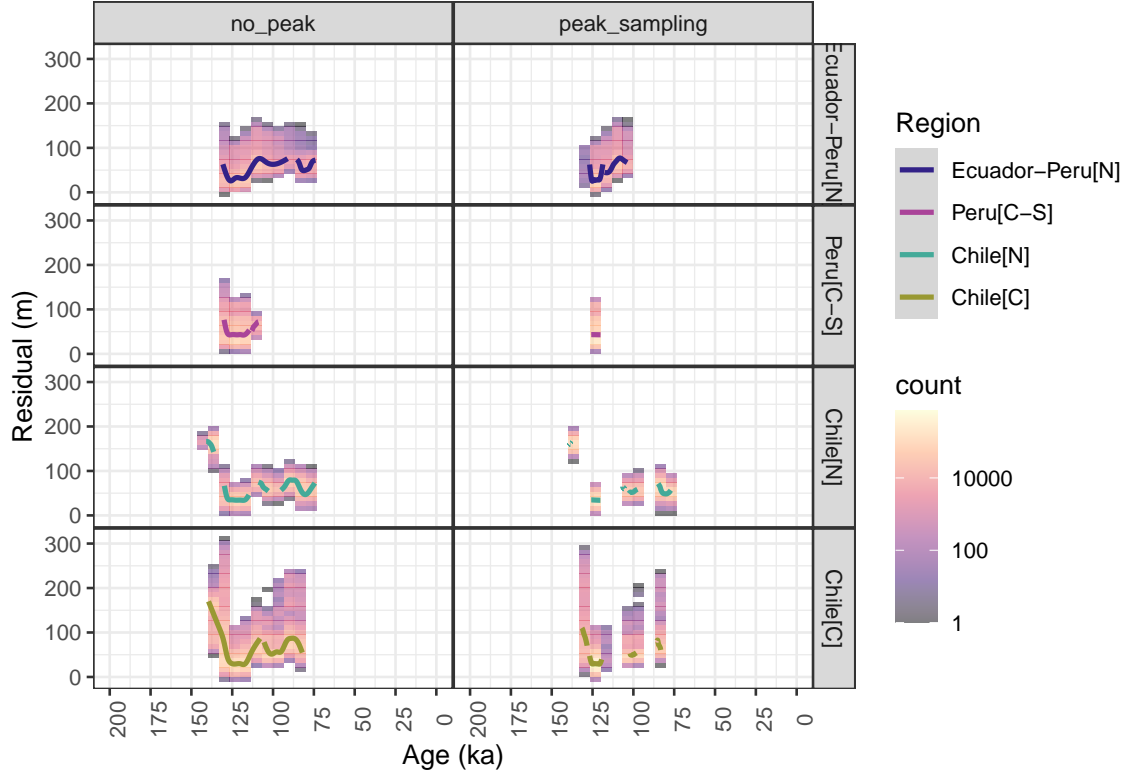


Figure 4.8: South American Pacific coast. Residual values by region and sampling method. Solid line correspond to fitted line. Bins represent number of points (point cloud) by age and residual value.

values resulting from different GIA model parameters, their geographic area, and specific GIA model configuration (see Table 4.2). The H_0 hypothesis for all tests is that the central tendency of all parameters is the same. H_1 for all cases is that central tendencies are different. Table 4.5 shows that for all cases the null hypothesis H_0 is rejected using a P-value of 0.05 (P-values lower than 0.05 in **bold**).

Table 4.5: South America Pacific coast - Kruskal test

Parameter	Degrees of freedom	No peak sampling		Peak sampling	
		$\tilde{\chi}^2$	P-value	$\tilde{\chi}^2$	P-value
Region	3	339932.3	P<0.001	821523.4	P<0.001
Propagation	1	19264.8	P<0.001	2026.3	P<0.001
Ice	2	438.7	P<0.001	1152.1	P<0.001
Lower mantle viscosity	5	53.4	P<0.001	50.4	P<0.001
Upper mantle viscosity	1	95.3	P<0.001	134.8	P<0.001
Lithospheric thickness	2	288.2	P<0.001	311.0	P<0.001
Model	215	20498.9	P<0.001	4153.0	P<0.001

A Pair-Wise Wilcoxon test was performed to identify the parameters, regions,

4. Results

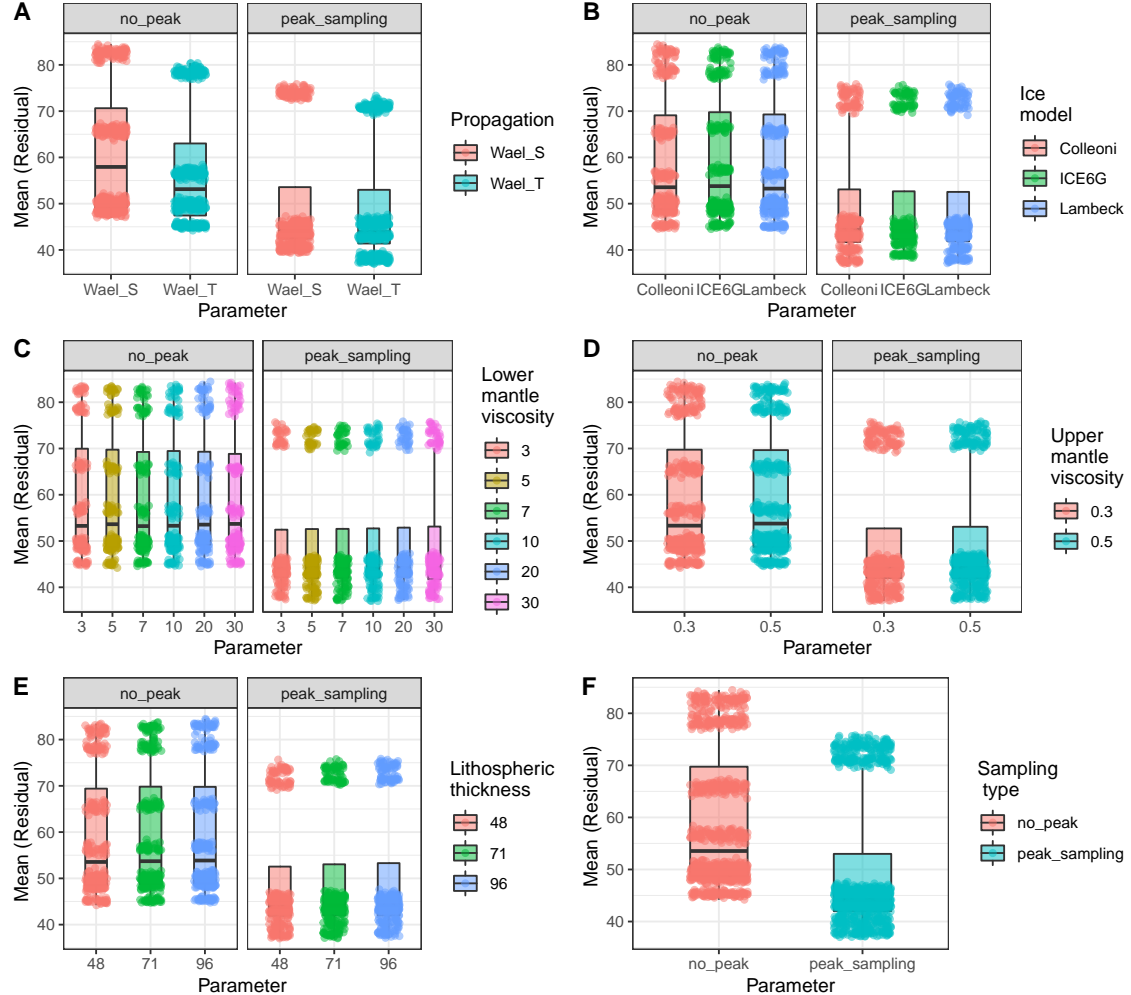


Figure 4.9: South American Pacific coast mean residual values by model parameters and sampling method.

or specific model that produces significantly different residual results. Table 4.6 shows the total of possible combinations (Pairs) for each grouping parameter and the number of pairs with statistically significant differences ($P\text{-value} < 0.05$) for their central tendencies. All combinations of regions have statistically significant differences for both sampling techniques. Similarly, all model parameters (except Lower mantle viscosity) have a high proportion of pairs (more than 50%) with significant differences in their central tendencies. Lastly, the pair-wise tests show that there is an important proportion of significantly different pairs of residual values by models (30% for *No-peak* and 52% for *Peak sampling*). That suggests that some models result in consistently different residual values.

As suggested by the Kruskal tests, central tendencies for different regions are different. Figure 4.10 shows the residual mean values grouped by region and sampling technique. As for the other grouping parameters, mean residual values

4. Results

Table 4.6: South America Pacific coast - Pairwise Wilcox test

Grouping parameter	Number of pairs	No peak sampling		Peak sampling	
		Significant different pairs	Significant different pairs	Significant different pairs	Significant different pairs
Region	6	6	6	6	6
Propagation	1	1	1	1	1
Ice	3	2	2	3	3
Lower mantle viscosity	15	8	8	7	7
Upper mantle viscosity	1	1	1	1	1
Lithospheric thickness	3	3	3	3	3
Model	23220	6888	6888	12236	12236

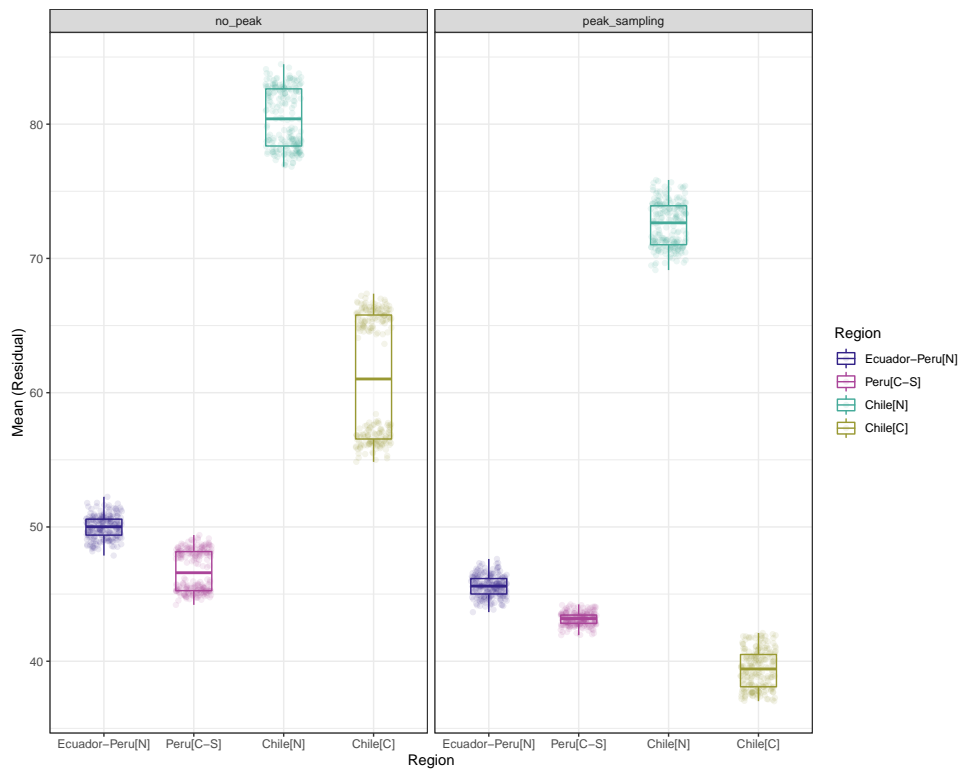


Figure 4.10: South American Pacific coast mean residual values by region.

from *Peak sampling* are in all cases lower than the ones resulting from *No-peak sampling*. For both sampling methods, the Ecuadorian and northern Peruvian coast (Ecuador-Peru[N]), the central Peruvian (Peru[C-S]), and the north Chilean coast (Chile[N]) coincide in their relative position. Chile[N] is the one with the highest mean residual values, followed by the Ecuador-Peru[N] and the Peru[C-S] area. However, the central Chilean region shows changes in its relative position by mean residual values. This region varies from the one with the second-highest mean values (around 60m) for the *No-peak sampling* to the one with the lowest mean values for the *Peak sampling* technique.

5

Discussion

Interpretations of residual values obtained in each case study require individual analysis based on the particular characteristics of the area. This includes the series of assumptions due to the geological characteristics of the regions, the context of the data (GIA models and SLIPs), and the methodology applied to perform the comparison. Therefore, despite the identical workflow, similar results could have different interpretations (e.g., mean residual values, Kruskal, and Wilcoxon tests).

5.1 South American Atlantic coast

For the South American Atlantic coast case study, the most important assumptions are that 1) relative sea level change in this region due to tectonic activity is negligible, and 2) GIA is the main driver of changes in relative sea level. In consequence, the contribution of some of the components that affect the changes on relative sea level changes could be considered equal to zero. That results in the following relationships derived from Equations (2.6) and (2.11):

$$\begin{aligned}\Delta RSL(\varphi, t) = & \Delta EUS(t) + \Delta ISO_{GIA}(\varphi, t) + \Delta ISO_{fingerprint}(\varphi, t) + \underline{\Delta TECT(\varphi, t)} \\ & + \underline{\Delta LOCAL(\varphi, t)} + \underline{\Delta UNSP(\varphi, t)}\end{aligned}\quad (5.1)$$

$$\varepsilon = \Delta RSL(\varphi, t) - \Delta ISO_{GIA}(\varphi, t) \quad (5.2)$$

5. Discussion

Under these assumptions, the Residual (ε) that results from the comparison of SLIPs (Point cloud) and GIA models in the South American Atlantic coast is equal to the sum of the (unknown) Eustatic ($\Delta EUS(t)$) and fingerprint ($\Delta ISO_{fingerprint}(\varphi, t)$) component.

$$\varepsilon = \Delta EUS(t) + \Delta ISO_{fingerprint}(\varphi, t) \quad (5.3)$$

As the Eustatic component ($\Delta EUS(t)$) is not spatially dependent, the Residual (ε) values from different regions should be relatively similar for different regions with variations due to the gravitational isostatic effect ($\Delta ISO_{fingerprint}(\varphi, t)$). Results from the *No-peak sampling* and *Peak sampling* methods for the four regions along the South American Atlantic coast (see Figure 4.3) show that, for periods where all regions have information (e.g., *No-peak sampling* at 130 to 70 ka), the residual values follow a similar trend with small variations. That may suggest that the assumption that the tectonic ($\Delta TECT(\varphi, t)$), local ($\Delta LOCAL(\varphi, t)$), and Unspecified ($\Delta UNSP(\varphi, t)$) effects are negligible is correct. This similar trend is also possible if the net effect of $\Delta TECT(\varphi, t)$, $\Delta LOCAL$, and $\Delta UNSP$ is not zero but equal for all regions. However, the latter scenario is improbable due to the geographical extent of the study. Under the assumption that these components are zero, the fingerprint ($\Delta ISO_{fingerprint}(\varphi, t)$) should be able to explain the variations on residual values. Although the fingerprint is not known for this study, the $\Delta ISO_{fingerprint}(\varphi, t)$ is sensitive to the distance of the melting ice sheet (see Hay et al., 2014), which in this case study varies from the Brazilian northeast to the Argentinian southeast coast and could potentially explain differences in the residuals.

The notion that all regions share a common trend with variations due to the $\Delta ISO_{fingerprint}(\varphi, t)$ might be contradictory to the results from the Kruskal and Wilcoxon tests (see Table 4.2 and Table 4.3) which suggest that all regions have different mean residual values. Although these differences by region are evident (see Figure 4.5), their explanation might not be due to geological reasons but to the context of the data analyzed in each region. While the Brazilian northeast coast only has SLIPs (Point cloud) with a high age density around 120 and 100 ka, other regions have a temporal extend (see *No-peak sampling*) from 175 to 80 ka. For the Argentinian southeast coast, the region has the highest residual mean values around 50m but is also the only region with residual values between 175 and 140 ka. For this period, residual values are above 100m, higher than other periods where all sub-regions have values. The difference of having a period recorded only

5. Discussion

by one region with high residual values drives up the average residual values for the Argentinian southeast coast. That supports the observation that different mean residual values result from the various periods compared and do not necessarily provide information of geologic relevance. Therefore, similar trends between the regions (fitted residual curves) and different mean residual values are compatible.

Beyond the differences of mean residual values by regions, the Kruskal and Wilcoxon tests suggested significant differences in residual values by GIA model parameters. For some parameters, such as the Lower Mantle viscosity, the number of significantly different pairs suggests that this parameter influences residual values. However, these differences are inconsistent for most model parameters between sampling methods (see Table 4.3). As exceptions, the number of significantly different pairs for lithospheric thickness and the specific model show some consistency between sampling methods. In particular, both sampling methods show that differences in the lithospheric thickness result in different residual values.

In contrast, both sampling methods show that no particular model (5 parameter combination) is consistently different from the other models. That observation could be explained as most of the SLIPs (Point cloud) for these regions have data between 140 ka and 0 ka, where GIA models values tend to have minor variations (see Figure 4.2). However, as mentioned in the Methodology, the Kruskal and Wilcoxon test results must be interpreted with caution as the residual values do not meet the independence assumption. For example, differences in the age range covered by each region's sea-level index points (SLIPs) affect the final mean residual values comparisons.

5.2 South American Pacific coast

As the South American Pacific coast shows active tectonics, the assumptions differ from the Atlantic case study. In particular, for the Pacific coast is no longer valid to assume that the tectonic effect ($\Delta TECT(\varphi, t)$) is negligible and that the GIA is the principal driver of sea-level changes. Consequently, for the Pacific coast, the following relationships apply:

$$\begin{aligned} \Delta RSL(\varphi, t) = & \Delta EUS(t) + \Delta ISO_{GIA}(\varphi, t) + \Delta ISO_{fingerprint}(\varphi, t) + \Delta TECT(\varphi, t) \\ & + \Delta LOCAL(\varphi, t) + \Delta UNSP(\varphi, t) \end{aligned} \quad (5.4)$$

$$\varepsilon = \Delta RSL(\varphi, t) - \Delta ISO_{GIA}(\varphi, t) \quad (5.5)$$

5. Discussion

$$\varepsilon = \Delta EUS(t) + \Delta ISO_{fingerprint}(\varphi, t) + \Delta TECT(\varphi, t) + \Delta LOCAL(\varphi, t) + \Delta UNSP(\varphi, t) \quad (5.6)$$

Under these assumptions, it is not expected to have similar residual values for different regions (like the Atlantic region) as more phenomena are involved in sea-level changes. The *No-peak sampling* and *peak sampling* methods for the four regions along the South American Pacific coast (see Figure 4.7) show similarities and differences with the Pacific area. On the one hand, similar to the Atlantic region, the GIA models show high variability between 200k and 130 ka and low variability between 130 and 0 ka. However, the Ecuadorian and north Peruvian (Ecuador-Peru[n]) region shows a relatively higher variability than the other regions. On the other hand, SLIPs (Point cloud) values are usually higher than in the Atlantic regions. For example, there are SLIPs in the Ecuador-Peru[N] and Chile[C] regions with relative sea level values higher than 50 m (and up to 200 m). That observation is consistent with the assumption that $\Delta TECT(\varphi, t)$ is not negligible, and observations of tectonic uplifting in the area resulted from other studies with the same data set of SLIPs (see Freisleben et al., 2021).

Despite the differences in SLIPs values, Residual (ε) values from high-density age ranges (see Figure 4.8) seem to follow a similar pattern. All regions coincide with a lowest residual value of around 40-50 m at 130 ka, being the Peruvian central and southern area (Peru[C-S]) slightly higher than the other regions. This might suggest that the net effect of the tectonic ($\Delta TECT(\varphi, t)$), local $\Delta LOCAL(\varphi, t)$ and $\Delta UNSP(\varphi, t)$ is similar between the different regions. An additional factor to consider is that local variations within each region are possible. Freisleben et al. (2021) shows that the elevation of marine terraces (i.e., Elevation parameter for Indicative Range calculation) across these four areas and its derived uplift rate is not constant. For example, the Peru[C-S] regions show marine terraces elevations up to 110 m while the median of all regions coincides around 30 m. Significant higher than the median elevation values occur in all regions as the Manta Peninsula (Ecuador-Peru[N] region), San Juan de Marcona (Peru[C-S]), Mejillones Peninsula (Chile[N]) and the Arauco Peninsula (Chile[C]) (see Freisleben et al., 2021). Although there are differences within each region, the observation that all regions share the same median elevation parameter for their marine terraces could explain why the residual values follow a similar trend.

As for the Atlantic case study, the similarity of trends in the fitted residual values for all Pacific regions seems to contradict differences in mean residual values

5. Discussion

by region. The northern Chilean coast (Chile[N]) has the highest mean residual value (for *No-peak sampling*) of around 80 m, while the Peruvian central and south coast (Peru[C-S]) have the lowest mean value around 47 m. In this case, the differences in the age range covered by each region play a role. For example, the Peru[C-S] region only has residual data from 130 to 110 ka for the *No-peak sampling* method. Other areas for the same sampling methods cover SLIPs from around 150 to 75 ka. In particular, the lower temporal constraint for the remaining regions varies from 145 ka for Chile [N], 140 ka for Chile[C], and 130 for Ecuador-Peru[N]. That difference in a period with relatively high residual values (more than 100 m) affects the resulting mean residual values.

Regarding the model parameters, the Kruskal and Wilcoxon tests suggest significant differences in residual values due to different model configurations in a consistent way for both sampling methods (see Table 4.6 and 4.5). In this case, the Propagation, Ice, Upper Mantle viscosity, and Lithospheric thickness parameters seem to produce consistently different residual values. The comparisons by a specific model (216 GIA models) for the Pacific region show a high number of statistically significant different pairs. That suggests a higher sensibility in residual values due to the GIA model in the Pacific than the Atlantic region. That observation is consistent with a higher number of SLIPs before 130 ka (e.g., Chile[N] and Chile[C]), where GIA models show a higher variability (see Figure 4.7). As more SLIPs are temporally located in an age range with higher GIA variability, resulting residual values are more sensitive to GIA models differences.

5.3 Sampling methods

Differences in the results due to sampling methods had been mentioned in the individual results and discussion by regions. However, general observations are valid for any studied region using these different approaches.

The first, and perhaps the most evident, is that more prominent differences between the methods are expected for regions with more SLIPs with uniform temporal constraints. For example, the northeast Brazilian coast (BR[NE]) has a low number of SLIPs with uniform distribution resulting in similar relative sea level Point clouds (see Figure 4.7 and Table 4.1) and consequently similar residual values. In the opposite case, high variations between sampling methods are expected for the south Brazilian coast (BR[S]), where most SLIPs have a uniform temporal constraint.

A second observation is that Point clouds for the *Peak sampling* method seem

5. Discussion

to cluster around local maximum and minimal relative sea level values from the GIA models. Although this behavior might be expected, it is relevant to reiterate that peak-sampling ranges are not defined using GIA models but a relative sea level stack based on proxies published by Spratt and Lisiecki (2016). This effect might be especially relevant in a region where GIA is the predominant sea-level change driver. GIA and relative sea level peaks would coincide in this particular case, enabling lower residual values. This observation is consistent with the mean values, Kruskal and Wilcoxon tests that show lower Residual values for the *Peak sampling* method.

Third, because of the SLIPs characteristics, *Peak sampling* results in multiple separate portions of information. As residual values are clustered around peaks, high-density age ranges are concentrated around particular periods. Different factors could explain the differences between the sampling methods results. The most important one is that the definition of a high-density age range is arbitrary (<15% of highest density) and might cause erroneously ignoring periods under some conditions. For example, if a specific temporal constraint is dominant because of the number of SLIPs in the region, other age constraints would always fall in the *low-density age range*. That is especially important for the Pacific study, where different SLIPs around the coast share the same temporal constraint from *Referencing points* for up to 600 km (see Freisleben et al., 2021, Methods). Similarly, because of the clustering around specific age ranges, intermediate values between peaks also fall into the *low-density age range* and thus are ignored for the curve fitting.

The combination of all effects has different results for each area depending on the context of the SLIPs analyzed. For seven out of eight comparisons between sampling techniques, the results seem to be consistent if compared the relative position of mean values by regions (see Figure 4.5 and Fig. 4.10). However, for the central Chilean coast (Chile[C]) - Fig. 4.10) difference in sampling methods show a high variation in mean residual values from being the second higher around 60 m for the *No-peak sampling* to be the smallest (around 40 m) for the *Peak sampling*. As discussed before, drastic changes could be explained by age ranges differences between the two methods for this region. In particular, Age ranges with high residual values (e.g., over 100 m before 130 ka) are ignored for the *Peak sampling* method, while they are included in the *No-peak sampling* method.

Results from the case studies and the comparison between sampling methods allow concluding on the initial research hypothesis of this study. On the one hand, a comparison between the Atlantic and Pacific region fitted residual curves confirm the initial hypothesis that the active Pacific margin has higher residual values than

5. Discussion

the passive Atlantic margin. Specifically, while the Pacific coast's residual values fluctuate between 30 to 100 m from 125 to 75 ka, the Atlantic passive margin varies from 0 to 50 m for the same period. As discussed before, this difference might indicate the presence of tectonic uplift only for the Pacific coast. On the other hand, a comparison between mean residual values by sub-regions (i.e., along the same coast) shows no information of geologic value. Mean residual values by sub-regions are affected by the temporal coverage of each region. Therefore, differences should not be interpreted as the result of geological processes.

6

Conclusions

Results from the proposed method for comparison allow general observations of both the studied areas and the comparison method.

First, comparing case studies between active and passive tectonic margins results in the expected behavior. Specifically, the South American Pacific coast, an active tectonic margin, shows higher residual values than the passive tectonic Atlantic coast. This observation results from comparing the fitted residual curves for all sub-regions where the ones located in the Pacific exhibit higher values for coinciding temporal ranges (e.g., Residual values around 125 ka) than the Atlantic areas. However, the results of both case studies suggest that comparison between regions requires analyzing the context of the compared area's data before reaching conclusions, as SLIPs are temporally and spatially irregular. For example, direct comparison using the mean residual values of areas is misleading as differences could result from different temporal covers instead of geological reasons. Even for regions where the spatial distribution of data is uniform (e.g., Pacific coast), other factors as the age correlation methods used to produce the SLIPs influence the resulting mean residual values.

Second, the use of different sampling techniques results in similar residual values. Despite differences in mean residual values between the *No-peak sampling* and *Peak sampling* methods, residual levels (fitted curve) for coinciding temporal ranges exhibit similar trends. As for the previous case, direct comparison of the techniques using mean residual values is incorrect as differences could be explained by different temporal extends. That is especially relevant as temporal ranges greatly vary

6. Conclusions

between the sampling methods for areas with a high number of SLIPs with uniform age distribution (i.e., MIS assignment). An important observation is that sampling techniques result in different temporal coverage of the residual values. In general, for *No-peak sampling*, the temporal coverage is more extended than the *Peak sampling* due to the higher temporal uncertainty of the SLIPs. Consequently, analysis of the residual with any sampling methods should verify if the assumption that SLIPs are preserved only in highstands (i.e., *Peak sampling*) is applicable.

The resulting limitations from the proposed methodology indicate required future research needs and open questions. First, further work applying this methodology should expand in statistical techniques that allow comparison between regions by handling differences in the spatial distribution, the number of sea-level indicators by area, age coverage differences, and the proportion of uniform ages (i.e., MIS assigned). A potential path to explore is including the ‘Quality of age’ and ‘Quality of RSL information’ parameter available for the age and RSL parameters to weigh the importance of an individual SLIP in the computation of regional residuals. Similarly, the implementation of a comparison of mean residual values for common age ranges covered by different regions could provide valuable information. Second, as the proposed methodology does not include limiting data for the analysis, additional work is required to incorporate all sea level indicators (i.e. SLIPs and limiting data) into the analysis. Third, it would require further research to evaluate the extent of residual variability resulting from the method’s random sampling techniques. Due to technical limitations and the computational complexity of the methodology, the study only includes a single iteration. Even though similar general conclusions are expected, the variation due to the random component should be studied.

Despite the limitations of the analysis, this work presents an approach to compute residual values by integrating and comparing sea-level change information from multiple origins in a reproducible workflow. This study makes both technical and methodological contributions to the study of sea-level changes. On the one hand, this work presents the implementation of the methods required to compare SLIPs and GIA models, and it handles technical details to facilitate the integration of sea-level information. For example, this work includes new ways to explore the WALIS data set and presents GIA model output (Dendy et al., 2017) as an 8-dimensional spatial cube instead of a series of 216 different files contributing to its standardization. As a result, other researchers could apply the method presented in any other region using the code that results from this work. This work tested the proposed method in different geological contexts, explored ways to analyze the resulting residual values,

6. Conclusions

discussed the limitations of the analysis, and proposed potential explanations for different results. An important aspect is that the methodology explores integrating previously excluded data as SLIPs with uniform (MIS Assigned / relative dating) temporal constraints into the statistical methods to analyze sea-level changes. The methodology proposed is built on top of previous efforts to standardize sea-level indicators and shows the potential and methodological and technical challenges to integrate sea-level information from different sources.

References

- M.L. Aguirre, D.Q. Bowen, G.A. Sykes, and R.C. Whatley. 1995. A provisional aminostratigraphical framework for late Quaternary marine deposits in Buenos Aires province, Argentina. *Marine Geology* 128, 1 (1995), 85–104. [https://doi.org/10.1016/0025-3227\(95\)00058-7](https://doi.org/10.1016/0025-3227(95)00058-7)
- M.L. Aguirre and R.C. Whatley. 1995. Late Quaternary marginal marine deposits and palaeoenvironments from northeastern Buenos Aires Province, Argentina: A review. *Quaternary Science Reviews* 14, 3 (1995), 223–254. [https://doi.org/10.1016/0277-3791\(95\)00009-E](https://doi.org/10.1016/0277-3791(95)00009-E)
- Miguel C Albero and Fernando E Angiolini. 1983. Ingeis Radiocarbon Laboratory Dates I. *Radiocarbon* 25, 3 (1983), 831–842. <https://doi.org/10.1017/S0033822200006238>
- Erica L Ashe, Niamh Cahill, Carling Hay, Nicole S Khan, Andrew Kemp, Simon E Engelhart, Benjamin P Horton, Andrew C Parnell, and Robert E Kopp. 2019. Statistical modeling of rates and trends in Holocene relative sea level. *Quaternary Science Reviews* 204 (2019), 58–77.
- L.M. Barbosa, A.C.S.P. Bittencourt, J.M.L. Dominguez, and Louis Martin. 1986. The Quaternary coastal deposits of the State of Alagoas : influence of the relative sea-level changes. In *Quaternary of south America and Antarctic peninsula*. A.A. Balkema, Rotterdam, 269–290. <https://www.documentation.ird.fr/hor/fdi:24777>
- Alcina Magnólia Franca Barreto, Francisco Hilário Rego Bezerra, Kenitiro Suguiio, Sonia Hatsue Tatumi, Marcio Yee, Rosemeire P. Paiva, and Casimiro S. Munita. 2002. Late Pleistocene marine terrace deposits in northeastern Brazil: sea-level change and tectonic implications. *Palaeogeography, Palaeoclimatology, Palaeoecology* 179, 1 (2002), 57–69. [https://doi.org/10.1016/S0031-0182\(01\)00408-4](https://doi.org/10.1016/S0031-0182(01)00408-4)
- Adelma Bayarsky and Jorge Osvaldo Codignotto. 1982. Pleistocene-Holocene marino en Puerto Lobos, Chubut. *Revista de la Asociación Geológica Argentina* 37, 1 (1982), 91–99.
- M. Bender, T. Mann, P. Stocchi, D. Kneer, T. Schöne, J. Illigner, J. Jompa, and A. Rovere. 2020. Late Holocene (0–6 ka) sea-level changes in the Makassar Strait, Indonesia. *Climate of the Past* 16, 4 (2020), 1187–1205. <https://doi.org/10.5194/cp-16-1187-2020>
- M. Bernat, Louis Martin, A. Bittencourt, and G. Vilas Boas. 1983. Datations Io-U du plus haut niveau marin du dernier interglaciaire sur la côte du Brésil : utilisation du 229Th comme traceur. *Comptes Rendus de l'Académie des Sciences de Paris. Série 2 : Mécanique...* 296 (1983), 197–200. <https://www.documentation.ird.fr/hor/fdi:41888>
- A.C.S.P. Bittencourt, Louis Martin, G.S. Vilas Boas, and J.M. Flexor. 1979. Quaternary marine formations of the coast of the state of Bahia (Brazil). In *International symposium on coastal evolution in the quaternary*. P. 232–253. <https://www.documentation.ird.fr/hor/fdi:41922>
- Svante Björck, Kurt Lambeck, Per Möller, Nicolas Waldmann, Ole Bennike, Hui Jiang, Dongling Li, Per Sandgren, Anne Birgitte Nielsen, and Charles T. Porter. 2021. Relative sea level changes and glacio-isostatic modelling in the Beagle Channel, Tierra del Fuego, Chile: Glacial and tectonic implications. *Quaternary Science Reviews* 251 (2021), 106657. <https://doi.org/10.1016/j.quascirev.2020.106657>
- Hans W. Borchers. 2021. *pracma: Practical Numerical Math Functions*. <https://CRAN.R-project.org/package=pracma> R package version 2.3.3.
- Gustavo Gabriel Bujalesky. 2007. Coastal geomorphology and evolution of Tierra del Fuego (Southern Argentina). *Geologica Acta: an international earth science journal* 5, 4 (2007), 337–362.
- Gustavo Gabriel Bujalesky, A Coronato, and Federico Ignacio Isla. 2001. Ambientes glacifluviales y litorales cuaternarios de la región del río Chico, Tierra del Fuego, Argentina. *Revista de la Asociación Geológica Argentina* 56, 1 (2001), 73–90.
- Gustavo Gabriel Bujalesky and Federico Ignacio Isla. 2006. Depósitos cuaternarios de la costa atlántica fueguina, entre los cabos Peñas y Ewan. *Revista de la Asociación Geológica Argentina* 61, 1 (ene. 2006), 81–92. <https://revista.geologica.org.ar/raga/article/view/1062>
- Niamh Cahill, Andrew C. Kemp, Benjamin P. Horton, and Andrew C. Parnell. 2015. Modeling sea-level change using errors-in-variables integrated Gaussian processes. *The Annals of Applied Statistics* 9, 2 (2015), 547 – 571. <https://doi.org/10.1214/15-AOAS824>

References

- C. Cerrone, M. Vacchi, A. Fontana, and A. Rovere. 2021. Last Interglacial sea-level proxies in the western Mediterranean. *Earth System Science Data* 13, 9 (2021), 4485–4527. <https://doi.org/10.5194/essd-13-4485-2021>
- P. M. Chutcharavan and A. Dutton. 2021. A global compilation of U-series-dated fossil coral sea-level indicators for the Last Interglacial period (Marine Isotope Stage 5e). *Earth System Science Data* 13, 7 (2021), 3155–3178. <https://doi.org/10.5194/essd-13-3155-2021>
- James A. Clark, William E. Farrell, and W. Richard Peltier. 1978. Global Changes in Postglacial Sea Level: A Numerical Calculation. *Quaternary Research* 9, 3 (1978), 265–287. [https://doi.org/10.1016/0033-5894\(78\)90033-9](https://doi.org/10.1016/0033-5894(78)90033-9)
- Jorge Osvaldo Codignotto. 1983. Depósitos elevados y/o de acreción Pleistoceno-Holoceno en la costa Fueguino-Patagónica. In *Símposio Oscilaciones del nivel del mar durante el último hemiciclo deglacial en la Argentina*. 12–26.
- K. M. Cohen, V. Cartelle, R. Barnett, F. S. Busschers, and N. L. M. Barlow. 2021. Last Interglacial sea-level data points from Northwest Europe. *Earth System Science Data Discussions* 2021 (2021), 1–75. <https://doi.org/10.5194/essd-2021-390>
- Jessica R. Creveling, Jerry X. Mitrovica, Peter U. Clark, Claire Waelbroeck, and Tamara Pico. 2017. Predicted bounds on peak global mean sea level during marine isotope stages 5a and 5c. *Quaternary Science Reviews* 163 (2017), 193–208. <https://doi.org/10.1016/j.quascirev.2017.03.003>
- S. Dendy, J. Austermann, J.R. Creveling, and J.X. Mitrovica. 2017. Sensitivity of Last Interglacial sea-level high stands to ice sheet configuration during Marine Isotope Stage 6. *Quaternary Science Reviews* 171 (2017), 234–244. <https://doi.org/10.1016/j.quascirev.2017.06.013>
- J.M Dominguez, ACSP Bittencourt, ZMAN Leão, and AEG Azevedo. 1990. Geologia do Quaternário costeiro do estado de Pernambuco. *Revista Brasileira de Geociências* 20, 2 (1990).
- J.F. Dumont, E. Santana, W. Vilema, K. Pedoja, M. Ordóñez, M. Cruz, N. Jiménez, and I. Zambrano. 2005. Morphological and microtectonic analysis of Quaternary deformation from Puná and Santa Clara Islands, Gulf of Guayaquil, Ecuador (South America). *Tectonophysics* 399, 1 (2005), 331–350. <https://doi.org/10.1016/j.tecto.2004.12.029> Andean Geodynamics..
- Blake Dyer, Jacqueline Austermann, William J. D'Andrea, Roger C. Creel, Michael R. Sandstrom, Miranda Cashman, Alessio Rovere, and Maureen E. Raymo. 2021. Sea-level trends across The Bahamas constrain peak last interglacial ice melt. *Proceedings of the National Academy of Sciences* 118, 33 (2021). <https://doi.org/10.1073/pnas.2026839118> arXiv:<https://www.pnas.org/content/118/33/e2026839118.full.pdf>
- WE Farrell and James A Clark. 1976. On postglacial sea level. *Geophysical Journal International* 46, 3 (1976), 647–667.
- Horn Filho and Norberto Olmiro. 2017. Roteiro geológico na planície costeira de Santa Catarina, Brasil.
- R. Freisleben, J. Jara-Muñoz, D. Melnick, J. M. Martínez, and M. R. Strecker. 2021. Marine terraces of the last interglacial period along the Pacific coast of South America (1N–40S). *Earth System Science Data* 13, 6 (2021), 2487–2513. <https://doi.org/10.5194/essd-13-2487-2021>
- E Fucks, ML Aguirre, E Schnack, G Erra, and N Ramos. 2006. Rasgos litológicos y fosilíferos de la Formación Pascua (Pleistoceno Tardío) en su localidad tipo, provincia de Buenos Aires. In *III Congreso Argentino de Cuaternario y Geomorfología*. 10–13.
- Enrique Eduardo Fucks, Enrique Jorge Schnack, and Marina Laura Aguirre. 2010. Nuevo ordenamiento estratigráfico de las secuencias marinas del sector continental de la Bahía Samborombón, provincia de Buenos Aires. *Revista de la Asociación Geológica Argentina* 67 (2010).
- Sebastian Garzón and Alessio Rovere. 2021. WALIS visualization interface (Version 1.0). <https://doi.org/10.5281/zenodo.4943541>
- Gabriel González, José Cembrano, Daniel Carrizo, Alejandro Macci, and Heinz Schneider. 2003. The link between forearc tectonics and Pliocene–Quaternary deformation of the Coastal Cordillera, northern Chile. *Journal of South American Earth Sciences* 16, 5 (2003), 321–342. [https://doi.org/10.1016/S0895-9811\(03\)00100-7](https://doi.org/10.1016/S0895-9811(03)00100-7)
- S. Gordillo, G. Cusminsky, E. Bernasconi, J.F. Ponce, J.O. Rabassa, and M. Pino. 2010. Pleistocene marine calcareous macro-and-microfossils of Navarino Island (Chile) as environmental proxies during the last interglacial in southern South America. *Quaternary International* 221, 1 (2010), 159–174. <https://doi.org/10.1016/j.quaint.2009.10.025> Quaternary Land–Ocean Interactions: Driving Mechanisms and Coastal Responses.
- Sandra Gordillo and Federico. I. Isla. 2011. Faunistic changes between the Middle/Late Pleistocene and the Holocene on the Atlantic coast of Tierra del Fuego: molluscan evidence. *Quaternary International* 233, 2 (2011), 101–112. <https://doi.org/10.1016/j.quaint.2010.06.006> Quaternary Floral and Faunal Assemblages: Ecological and Taphonomical Investigations.

References

- E. J. Gowan, A. Rovere, D. D. Ryan, S. Richiano, A. Montes, M. Pappalardo, and M. L. Aguirre. 2021. Last interglacial (MIS 5e) sea-level proxies in southeastern South America. *Earth System Science Data* 13, 1 (2021), 171–197. <https://doi.org/10.5194/essd-13-171-2021>
- José Luis Goy, José Macharé, Luc Ortíeb, and Cari Zazo. 1992. Quaternary shorelines in southern Peru: A record of global sea-level fluctuations and tectonic uplift in Chala Bay. *Quaternary International* 15–16 (1992), 99–112. [https://doi.org/10.1016/1040-6182\(92\)90039-5](https://doi.org/10.1016/1040-6182(92)90039-5)
- A. J. Hartley and E. J. Jolley. 1995. Tectonic implications of Late Cenozoic sedimentation from the Coastal Cordillera of northern Chile (22–24°S). *Journal of the Geological Society* 152, 1 (02 1995), 51–63. <https://doi.org/10.1144/gsjgs.152.1.0051> arXiv:<https://pubs.geoscienceworld.org/jgs/article-pdf/152/1/51/4889907/gsjgs.152.1.0051.pdf>
- Carling Hay, Jerry X. Mitrovica, Natalya Gomez, Jessica R. Creveling, Jacqueline Austermann, and Robert E. Kopp. 2014. The sea-level fingerprints of ice-sheet collapse during interglacial periods. *Quaternary Science Reviews* 87 (2014), 60–69. <https://doi.org/10.1016/j.quascirev.2013.12.022>
- Marc P. Hijma, Simon E. Engelhart, Torbjörn E. Törnqvist, Benjamin P. Horton, Ping Hu, and David F. Hill. 2015. *A protocol for a geological sea-level database*. John Wiley & Sons, Ltd, Chapter 34, 536–553. <https://doi.org/10.1002/9781118452547.ch34> arXiv:<https://onlinelibrary.wiley.com/doi/pdf/10.1002/9781118452547.ch34>
- Norberto Olmiro Horn Filho and Daniel Higuera Simó. 2008. The upper pleistocene of São Francisco do Sul Island coastal plain: geomorphologic, sedimentologic and evolutive aspects. *Brazilian Journal of Oceanography* 56 (2008), 179–187.
- Jeffrey T. Hsu. 1992. Quaternary uplift of the peruvian coast related to the subduction of the Nazca Ridge: 13.5 to 15.6 degrees south latitude. *Quaternary International* 15–16 (1992), 87–97. [https://doi.org/10.1016/1040-6182\(92\)90038-4](https://doi.org/10.1016/1040-6182(92)90038-4)
- Jeffrey T. Hsu, Eric M. Leonard, and John F. Wehmiller. 1989. Aminostratigraphy of Peruvian and Chilean Quaternary marine terraces. *Quaternary Science Reviews* 8, 3 (1989), 255–262. [https://doi.org/10.1016/0277-3791\(89\)90040-1](https://doi.org/10.1016/0277-3791(89)90040-1)
- Martín Iriondo. 1994. The Quaternary of Ecuador. *Quaternary International* 21 (1994), 101–112. [https://doi.org/10.1016/1040-6182\(94\)90024-8](https://doi.org/10.1016/1040-6182(94)90024-8)
- Federico Ignacio Isla and Rodolfo José Angulo. 2015. Tectonic Processes along the South America Coastline Derived from Quaternary Marine Terraces. *Journal of Coastal Research* 32, 4 (04 2015), 840–852. <https://doi.org/10.2112/JCOASTRES-D-14-00178.1> arXiv:https://meridian.allenpress.com/jcr/article-pdf/32/4/840/2065051/jcoastres-d-14-00178_1.pdf
- Federico Ignacio Isla, NW Rutter, Enrique J Schnack, and Marcelo Zárate. 2000. La transgresión belgranense en Buenos Aires. *Publicación especial. Asociación Geológica Argentina. Serie D* 4 (2000).
- Thomas F Jamieson. 1865. On the history of the last geological changes in Scotland. *Quarterly Journal of the Geological Society* 21, 1-2 (1865), 161–204.
- Julius Jara-Muñoz, Daniel Melnick, Dominik Brill, and Manfred R. Strecker. 2015. Segmentation of the 2010 Maule Chile earthquake rupture from a joint analysis of uplifted marine terraces and seismic-cycle deformation patterns. *Quaternary Science Reviews* 113 (2015), 171–192. <https://doi.org/10.1016/j.quascirev.2015.01.005> Megathrust Earthquakes and Sea-level Change: a Tribute to George Plafker.
- Erick M Leonard and John F Wehmiller. 1991. Geochronology of marine terraces at Caleta Michilla, northern Chile; implications for Late Pleistocene and Holocene uplift. *Andean Geology* 18, 1 (1991), 81–86.
- Erick M Leonard and John F. Wehmiller. 1992. Low uplift rates and terrace reoccupation inferred from mollusk aminostratigraphy, Coquimbo Bay area, Chile. *Quaternary Research* 38, 2 (1992), 246–259. [https://doi.org/10.1016/0033-5894\(92\)90060-V](https://doi.org/10.1016/0033-5894(92)90060-V)
- Ulrik Lyngs. 2019. oxforddown: An Oxford University Thesis Template for R Markdown. <https://github.com/ulyngs/oxforddown>. <https://doi.org/10.5281/zenodo.3484681>
- José Macharé and Luc Ortíeb. 1992. Plio-Quaternary vertical motions and the subduction of the Nazca Ridge, central coast of Peru. *Tectonophysics* 205, 1 (1992), 97–108. [https://doi.org/10.1016/0040-1951\(92\)90420-B](https://doi.org/10.1016/0040-1951(92)90420-B) Andean geodynamics.
- Jose Macharé and L. Ortíeb. 1994. Morfoestratigrafía de los tablazos del norte de Perú: Neotectónica y fluctuaciones del nivel del mar, paper presented at VIII Congreso Peruano de Geología. *Soc. Geol. del Perú, Lima* (1994).
- Carlos Marquardt, Alain Lavenu, Luc Ortíeb, Estanislao Godoy, and Diana Comte. 2004. Coastal neotectonics in Southern Central Andes: uplift and deformation of marine terraces in Northern Chile (27°S). *Tectonophysics* 394, 3 (2004), 193–219. <https://doi.org/10.1016/j.tecto.2004.07.059>

References

- Louis Martin. 1982. Primeira ocorrencia de corais pleistocenicos da costa brasileira : datacao do maximo da penultima transgressao. *Ciencias da Terra* (1982), 16–17. <https://www.documentation.ird.fr/hor/fdi:010056860>
- Louis Martin and K. Suguio. 1976. Etude préliminaire du quaternaire marin : comparaison du littoral de São-Paulo et de Salvador de Bahia (Brésil). *Cahiers ORSTOM.Série Géologie* 8 (1976), 33–47. <https://www.documentation.ird.fr/hor/fdi:17139>
- Louis Martin, K. Suguio, and J.M. Flexor. 1979. Le quaternaire marin du littoral brésilien entre Cananeia (SP) et Barra de Guaratiba (RJ). In *International symposium on coastal evolution in the quaternary*. P. 296–331. <https://www.documentation.ird.fr/hor/fdi:41917>
- Louis Martin, Kenitiro Suguio, and Jean-Marie Flexor. 1988. Hauts niveaux marins Pleistocenes du littoral bresiliens. *Palaeogeography, Palaeoclimatology, Palaeoecology* 68, 2 (1988), 231–239. [https://doi.org/10.1016/0031-0182\(88\)90042-9](https://doi.org/10.1016/0031-0182(88)90042-9) Quaternary Coastal Changes.
- Joseph Martinod, Vincent Regard, Rodrigo Riquelme, German Aguilar, Benjamin Guillaume, Sébastien Carretier, Joaquín Cortés-Aranda, Laetitia Leanni, and Gérard Hérail. 2016. Pleistocene uplift, climate and morphological segmentation of the Northern Chile coasts (24°S–32°S): Insights from cosmogenic 10Be dating of paleoshorelines. *Geomorphology* 274 (2016), 78–91. <https://doi.org/10.1016/j.geomorph.2016.09.010>
- Danyelly Caetano Martins, Rodrigo R. Cancelli, Renato Pereira Lopes, Patricia Hadler, Erick H. Testa, and Eduardo Guimaraes Barbosa. 2018. Ocorrência de Ophiomorpha nodosa em sedimentos pleistocénicos da Planície Costeira da Pinheira, Santa Catarina, Brasil. *Revista Brasileira de Paleontologia* 21, 1 (2018), 79–86.
- Daniel Melnick, Bodo Bookhagen, Manfred R. Strecker, and Helmut P. Echtler. 2009. Segmentation of megathrust rupture zones from fore-arc deformation patterns over hundreds to millions of years, Arauco peninsula, Chile. *Journal of Geophysical Research: Solid Earth* 114, B1 (2009).
- Glenn A. Milne. 2015. *Glacial isostatic adjustment*. John Wiley & Sons, Ltd, Chapter 28, 419–437. <https://doi.org/10.1002/9781118452547.ch28> arXiv:<https://onlinelibrary.wiley.com/doi/10.1002/9781118452547.ch28>
- Jerry X. Mitrovica and Glenn A. Milne. 2003. On post-glacial sea level: I. General theory. *Geophysical Journal International* 154, 2 (08 2003), 253–267. <https://doi.org/10.1046/j.1365-246X.2003.01942.x> arXiv:<https://academic.oup.com/gji/article-pdf/154/2/253/1665900/154-2-253.pdf>
- Luc Ortlieb, B. Ghaleb, C. Hillaire Marcel, J. Machare, and P. Pichet. 1991. Geocronología de terrazas marinas en la costa sur-peruana : enfoque metodológico. In *Septimo congreso peruano de geología : volumen de resumenes extendidos*. 511–516. <https://www.documentation.ird.fr/hor/fdi:34903>
- Luc Ortlieb, J.L. Goy, C. Zazo, C. Hillaire Marcel, and G. Vargas. 1995. Late quaternary coastal changes in Northern Chile : guidebook for a fieldtrip (Antofagasta-Iquique, 23–25 november 1995). In *International geological correlation program : project 367 : late quaternary coastal records of rapid change : applications to present and future conditions : 2nd annual meeting : abstracts*. 177. <https://www.documentation.ird.fr/hor/fdi:010014794>
- Luc Ortlieb and J. Macharé. 1990. Quaternary marine terraces on the peruvian coast and recent vertical motions. In *Symposium international "Géodynamique andine" : résumés des communications*. 95–98. <https://www.documentation.ird.fr/hor/fdi:30999>
- L. Ortlieb, C. Zazo, J.L. Goy, C. Dabrio, and J. Macharé. 1996. Pampa del Palo: an anomalous composite marine terrace on the uprising coast of southern Peru. *Journal of South American Earth Sciences* 9, 5 (1996), 367–379. [https://doi.org/10.1016/S0895-9811\(96\)00020-X](https://doi.org/10.1016/S0895-9811(96)00020-X)
- Yoko Ota, Takahiro Miyauchi, Roland Paskoff, and Motoharu Koba. 1995. Plio-Quaternary marine terraces and their deformation along the Altos de Talinay, north-central Chile. *Andean Geology* 22, 1 (1995), 89–102.
- Marta Pappalardo, Marina Aguirre, Monica Bini, Ilaria Consoloni, Enrique Fucks, John Hellstrom, Ilaria Isola, Adriano Ribolini, and Giovanni Zanchetta. 2015. Coastal landscape evolution and sea-level change: a case study from Central Patagonia (Argentina). *Zeitschrift für Geomorphologie* 59, 2 (06 2015), 145–172. <https://doi.org/10.1127/0372-8854/2014/0142>
- Roland Paskoff. 1991. Likely occurrence of a mega-tsunami in the Middle Pleistocene, near Coquimbo, Chile. *Andean Geology* 18, 1 (1991), 87–91.
- Roland P. Paskoff. 1977. Quaternary of Chile: The State of Research. *Quaternary Research* 8, 1 (1977), 2–31. [https://doi.org/10.1016/0033-5894\(77\)90054-0](https://doi.org/10.1016/0033-5894(77)90054-0)
- Kevin Pedoja. 2003. Les terrasses marines de la marge Nord andine (Equateur et Nord Pérou): relations avec le contexte géodynamique. (2003).
- K. Pedoja, J.F. Dumont, M. Lamothe, L. Ortlieb, J.-Y. Collot, B. Ghaleb, M. Auclair, V. Alvarez, and B. Labrousse. 2006a. Plio-Quaternary uplift of the Manta Peninsula and La Plata Island and the subduction of the Carnegie Ridge, central coast of Ecuador. *Journal of South American Earth Sciences* 22, 1 (2006), 1–21. <https://doi.org/10.1016/j.jsames.2006.08.003>

References

- K. Pedoja, Jean-François Dumont, and Luc Ortlieb. 2009. Levantamiento cuaternario costero del Arco de Talara (Ecuador y norte del Perú): cuantificaciones con las secuencias de terrazas marinas. In *Geología y geofísica marina y terrestre del Ecuador : desde la costa continental hasta las Islas Galápagos*. CNDM ; IRD ; INOCAR, Guayaquil (ECU) ; Marseille (FRA) ; Guayaquil, 107–129. <https://www.documentation.ird.fr/hor/fdi:010051356>
- K. Pedoja, L. Ortlieb, J.F. Dumont, M. Lamothe, B. Ghaleb, M. Auclair, and B. Labrousse. 2006b. Quaternary coastal uplift along the Talara Arc (Ecuador, Northern Peru) from new marine terrace data. *Marine Geology* 228, 1 (2006), 73–91. <https://doi.org/10.1016/j.margeo.2006.01.004>
- W Richard Peltier. 2004. Global glacial isostasy and the surface of the ice-age Earth: the ICE-5G (VM2) model and GRACE. *Annu. Rev. Earth Planet. Sci.* 32 (2004), 111–149.
- Marco Pfeiffer, Jacobus P. Le Roux, Elizabeth Solleiro-Rebolledo, Helga Kemnitz, Sergey Sedov, and Oscar Seguel. 2011. Preservation of beach ridges due to pedogenic calcrete development in the Tongoy palaeobay, North-Central Chile. *Geomorphology* 132, 3 (2011), 234–248. <https://doi.org/10.1016/j.geomorph.2011.05.012>
- M Pino, K Moreno, and M Paz Riedemann. 2002. La terraza del ultimo interglacial en la costa de Valdivia: observaciones, interpretaciones y desafíos. In *Simposio Internacional de Geología Ambiental para Planificación del Uso del Territorio*. 165–169.
- G. Poepeau, E. Soliani JR, A. Rivera, E. LOSS, and M. VASCONCELLOS. 1988. Datação por termoluminescência de alguns depósitos arenosos costeiros do último ciclo climático, no Nordeste do Rio Grande do Sul. *Pesquisas em Geociências* 21, 21 (1988), 25–47. <https://doi.org/10.22456/1807-9806.21464>
- J. Quezada, G. González, T.J. Dunai, A. Jensen, and J. Juez-Larré. 2007. Alzamiento litoral Pleistoceno del Norte de Chile: edades 21Ne de la terraza costera más alta del área de Caldera-Bahía Inglesa. *Revista Geologica de Chile* 34, 1 (2007). <https://doi.org/10.4067/S0716-02082007000100005>
- Jorge Rabassa, Sandra Gordillo, Carlos Ocampo, and P Rivas Hurtado. 2008. The southernmost evidence for an interglacial transgression (Sangamon?) in South America. First record of upraised Pleistocene marine deposits in Isla Navarino (Beagle Channel, Southern Chile). *Geologica Acta* 6, 3 (2008), 251–258.
- Ulrich Radtke. 1987. Palaeo sea levels and discrimination of the last and the penultimate interglacial fossiliferous deposits by absolute dating methods and geomorphological investigations illustrated from marine terraces in Chile. *Berliner Geographische Studien* 25, 3 (1987), 13–342.
- Ulrich Radtke. 1989. Marine Terrassen und Korallenriffe-Das Problem der quartären Meeresspiegelschwankungen erläutert an Fallstudien aus Chile, Argentinien und Barbados. Terrasses marines et récifs coralliens-Le problème des variations du niveau de la mer au Quaternaire expliqué grâce à des exemples du Chili, de l'Argentine et de la Barbade. *Düsseldorfer Geographische Schriften* 27 (1989).
- Vincent Regard, Marianne Saillard, Joseph Martinod, Laurence Audin, Sébastien Carretier, Kevin Pedoja, Rodrigo Riquelme, Paola Paredes, and Gérard Héral. 2010. Renewed uplift of the Central Andes Forearc revealed by coastal evolution during the Quaternary. *Earth and Planetary Science Letters* 297, 1 (2010), 199–210. <https://doi.org/10.1016/j.epsl.2010.06.020>
- K. Rostami, W.R. Peltier, and A. Mangini. 2000. Quaternary marine terraces, sea-level changes and uplift history of Patagonia, Argentina: comparisons with predictions of the ICE-4G (VM2) model of the global process of glacial isostatic adjustment. *Quaternary Science Reviews* 19, 14 (2000), 1495–1525. [https://doi.org/10.1016/S0277-3791\(00\)00075-5](https://doi.org/10.1016/S0277-3791(00)00075-5)
- Alessio Rovere, Maureen E. Raymo, Matteo Vacchi, Thomas Lorscheid, Paolo Stocchi, Lluís Gómez-Pujol, Daniel L. Harris, Elisa Casella, Michael J. O’Leary, and Paul J. Hearty. 2016a. The analysis of Last Interglacial (MIS 5e) relative sea-level indicators: Reconstructing sea-level in a warmer world. *Earth-Science Reviews* 159 (2016), 404–427. <https://doi.org/10.1016/j.earscirev.2016.06.006>
- Alessio Rovere, Deirdre Ryan, Colin Murray-Wallace, Alexander Simms, Matteo Vacchi, Andrea Dutton, Thomas Lorscheid, Peter Chutcharavan, Dominik Brill, Melanie Bartz, Nathan Jankowski, Daniela Mueller, Kim Cohen, and Evan Gowan. 2020. Descriptions of database fields for the World Atlas of Last Interglacial Shorelines (WALIS). <https://doi.org/10.5281/zenodo.3961544>
- Alessio Rovere, Deirdre D Ryan, Colin Murray-Wallace, Alexander Simms, Matteo Vacchi, Andrea Dutton, Thomas Lorscheid, PM Chutcharavan, Dominik Brill, Melanie Bartz, et al. 2019. The World Atlas of Last Interglacial Shorelines (WALIS)-an ongoing research effort to standardize sea-level proxy data from the Last Interglacial. In *AGU Fall Meeting Abstracts*, Vol. 2019. PP31C–1649.
- Alessio Rovere, Paolo Stocchi, and Matteo Vacchi. 2016b. Eustatic and Relative Sea Level Changes. *Current Climate Change Reports* 2, 4 (2016), 221–231. <https://doi.org/10.1007/s40641-016-0045-7>
- Keven Roy and W.R. Peltier. 2015. Glacial isostatic adjustment, relative sea level history and mantle viscosity: reconciling relative sea level model predictions for the U.S. East coast with geological constraints. *Geophysical Journal International* 201, 2 (03 2015), 1156–1181. <https://doi.org/10.1093/gji/ggv066> arXiv:<https://academic.oup.com/gji/article-pdf/201/2/1156/17368448/ggv066.pdf>

References

- K. Rubio-Sandoval, A. Rovere, C. Cerrone, P. Stocchi, T. Lorscheid, T. Felis, A.-K. Petersen, and D. D. Ryan. 2021. A review of last interglacial sea-level proxies in the western Atlantic and southwestern Caribbean, from Brazil to Honduras. *Earth System Science Data* 13, 10 (2021), 4819–4845. <https://doi.org/10.5194/essd-13-4819-2021>
- Nat Rutter, Ulrich Radtke, and Enrique J. Schnack. 1990. Comparison of ESR and Amino Acid Data in Correlating and Dating Quaternary Shorelines along the Patagonian Coast, Argentina. *Journal of Coastal Research* 6, 2 (1990), 391–411. <http://www.jstor.org/stable/4297690>
- Nat Rutter, Enrique J. Schnack, Julio del Rio, Jorge L. Fasano, Federico I. Isla, and Ulrich Radtke. 1989. Correlation and dating of Quaternary littoral zones along the Patagonian coast, Argentina. *Quaternary Science Reviews* 8, 3 (1989), 213–234. [https://doi.org/10.1016/0277-3791\(89\)90038-3](https://doi.org/10.1016/0277-3791(89)90038-3)
- Marianne Saillard. 2008. *Dynamique du soulèvement côtier Pléistocène des Andes centrales: Etude de l'évolution géomorphologique et datations (10Be) de séquences de terrasses marines (Sud Pérou-Nord Chili)*. Ph.D. Dissertation. Université Paul Sabatier-Toulouse III.
- M. Saillard, S.R. Hall, L. Audin, D.L. Farber, G. Héral, J. Martinod, V. Regard, R.C. Finkel, and F. Bondoux. 2009. Non-steady long-term uplift rates and Pleistocene marine terrace development along the Andean margin of Chile (31°S) inferred from 10Be dating. *Earth and Planetary Science Letters* 277, 1 (2009), 50–63. <https://doi.org/10.1016/j.epsl.2008.09.039>
- M. Saillard, S.R. Hall, L. Audin, D.L. Farber, V. Regard, and G. Héral. 2011. Andean coastal uplift and active tectonics in southern Peru: 10Be surface exposure dating of differentially uplifted marine terrace sequences (San Juan de Marcona, 15.4°S). *Geomorphology* 128, 3 (2011), 178–190. <https://doi.org/10.1016/j.geomorph.2011.01.004>
- M. Saillard, J. Riotte, V. Regard, A. Violette, G. Héral, L. Audin, and R. Riquelme. 2012. Beach ridges U–Th dating in Tongoy bay and tectonic implications for a peninsula–bay system, Chile. *Journal of South American Earth Sciences* 40 (2012), 77–84. <https://doi.org/10.1016/j.jsames.2012.09.001>
- Gerhard Schellmann. 1998. *Jungkänozoische Landschaftsgeschichte Patagoniens (Argentinien): andine Vorlandvergletscherungen, Talentwicklung und marine Terrassen* (1. auflage ed.). Essener geographische Arbeiten, Vol. 29. Klartext, Essen. Teilw. zugl.: Essen, Univ., Habil.-Schr. 1997 u.d.T.: Schellmann, Gerhard: Andine Vorlandvergletscherungen und marine Terrassen.
- Gerhard Schellmann and Ulrich Radtke. 1997. Electron spin resonance (ESR) techniques applied to mollusc shells from South America (Chile, Argentina) and implications for palaeo sea-level curve. *Quaternary Science Reviews* 16, 3 (1997), 465–475. [https://doi.org/10.1016/S0277-3791\(96\)00104-7](https://doi.org/10.1016/S0277-3791(96)00104-7)
- Gerhard Schellmann and Ulrich Radtke. 1999. Problems encountered in the determination of dose and dose rate in ESR dating of mollusc shells. *Quaternary Science Reviews* 18, 13 (1999), 1515–1527. [https://doi.org/10.1016/S0277-3791\(99\)00043-8](https://doi.org/10.1016/S0277-3791(99)00043-8)
- Gerhard Schellmann and Ulrich Radtke. 2000. ESR dating stratigraphically well-constrained marine terraces along the Patagonian Atlantic coast (Argentina). *Quaternary International* 68–71 (2000), 261–273. [https://doi.org/10.1016/S1040-6182\(00\)00049-5](https://doi.org/10.1016/S1040-6182(00)00049-5) Nat Rutter Honararium.
- Ian Shennan. 2015. *Handbook of sea-level research*. John Wiley & Sons, Ltd, Chapter 2, 3–25. <https://doi.org/10.1002/9781118452547.ch2> arXiv:<https://arxiv.org/abs/https://onlinelibrary.wiley.com/doi/10.1002/9781118452547.ch2>
- Ian Shennan, Antony J Long, and Benjamin P Horton. 2015. *Handbook of sea-level research*. John Wiley & Sons, Ltd.
- G. Spada and D. Melini. 2019. SELEN⁴ (SELEN version 4.0): a Fortran program for solving the gravitationally and topographically self-consistent sea-level equation in glacial isostatic adjustment modeling. *Geoscientific Model Development* 12, 12 (2019), 5055–5075. <https://doi.org/10.5194/gmd-12-5055-2019>
- R. M. Spratt and L. E. Lisiecki. 2016. A Late Pleistocene sea level stack. *Climate of the Past* 12, 4 (2016), 1079–1092. <https://doi.org/10.5194/cp-12-1079-2016>
- Kenitiro Suguio, Francisco HR Bezerra, and Alcina MF Barreto. 2011. Luminescence dated Late Pleistocene wave-built terraces in northeastern Brazil. *Anais da Academia Brasileira de Ciências* 83 (2011), 907–920.
- Kenitiro Suguio, Louis Martin, Abílio CSP Bittencourt, Jose ML Dominguez, Jean-Marie Flexor, and Antonio EG De Azevedo. 1985. Flutuações do nível relativo do mar durante o Quaternário Superior ao longo do litoral brasileiro e suas implicações na sedimentação costeira. *Revista Brasileira de Geociências* 15, 4 (1985), 273–286.
- Kenitiro Suguio, Louis Martin, and Jose ML Dominguez. 1982. Evolução da planicie costeira do rio Doce (ES) durante o quaternário : influencia das flutuações do nível do mar. In *Atas do quarto simposio do quaternário no Brasil*. 93–116. <https://www.documentation.ird.fr/hor/fdi:41924>
- Kenitiro Suguio and Setembrino Petri. 1973. Stratigraphy of the Iguapé-Cananéia lagoonal region sedimentary deposits, São Paulo State, Brazil: part I: field observations and grain size analysis. *Boletim IG* 4 (1973), 01–20.

References

- Kenitiro Suguio, Sonia H Tatumi, Emilia A Kowata, Casimiro S Munita, and Rosemeire P Paiva. 2003. Upper Pleistocene deposits of the Comprida Island (Sao Paulo State) dated by thermoluminescence method. *Anais da Academia Brasileira de Ciencias* 75, 1 (2003), 91–96.
- S. B. Thompson and J. R. Creveling. 2021. A global database of marine isotope substage 5a and 5c marine terraces and paleoshoreline indicators. *Earth System Science Data* 13, 7 (2021), 3467–3490. <https://doi.org/10.5194/essd-13-3467-2021>
- Luiz J. Tomazelli, S.R. Dillenburg, and J.A. Villwock. 2006. Geological Evolution of Rio Grande do Sul Coastal Plain, Southern Brazil. *Journal of Coastal Research* (2006), 275–278. <http://www.jstor.org/stable/25741577>
- Luiz J. Tomazelli and Sergio R. Dillenburg. 2007. Sedimentary facies and stratigraphy of a last interglacial coastal barrier in south Brazil. *Marine Geology* 244, 1 (2007), 33–45. <https://doi.org/10.1016/j.margeo.2007.06.002>
- Gabriel Vargas and Luc Ortlieb. 1998. Patrones de variaciones climáticas durante el Cuaternario tardío en la costa de la Región de Antofagasta, Chile. *Bulletin de l'Institut français d'études andines* 27, 3 (1998).
- Pia Victor, Monika Sobiesiak, Johannes Glodny, SN Nielsen, and Onno Oncken. 2011. Long-term persistence of subduction earthquake segment boundaries: Evidence from Mejillones Peninsula, northern Chile. *Journal of Geophysical Research: Solid Earth* 116, B2 (2011).
- MP Villalobos and M Pino. 2005. *Evidencias de la fluctuación del nivel del mar y alzamientos tectónicos desde el Pleistoceno tardío en Isla Mancera X Región de Los Lagos-Chile: registro estratigráfico y sedimentológico*. Ph.D. Dissertation. Doctoral Thesis. Universidad Austral de Chile, Facultad de Ciencias, Escuela
- Jorge Villwock. 1984. Geology of the Coastal Province of Rio Grande do Sul, Southern Brazil. A Synthesis. *Pesquisas em Geociências* 16, 16 (1984), 5–49. <https://doi.org/10.22456/1807-9806.21711>
- Sarah A. Woodroffe and Natasha L. M. Barlow. 2015. *Reference water level and tidal datum*. John Wiley & Sons, Ltd, Chapter 11, 171–180. <https://doi.org/10.1002/9781118452547.ch11> arXiv:<https://onlinelibrary.wiley.com/doi/pdf/10.1002/9781118452547.ch11>
- Cari Zazo. 1999. Interglacial sea levels. *Quaternary International* 55, 1 (1999), 101–113. [https://doi.org/10.1016/S1040-6182\(98\)00031-7](https://doi.org/10.1016/S1040-6182(98)00031-7)